

We are IntechOpen, the world's leading publisher of Open Access books Built by scientists, for scientists

6,900

Open access books available

185,000

International authors and editors

200M

Downloads

Our authors are among the

154

Countries delivered to

TOP 1%

most cited scientists

12.2%

Contributors from top 500 universities



WEB OF SCIENCE™

Selection of our books indexed in the Book Citation Index
in Web of Science™ Core Collection (BKCI)

Interested in publishing with us?
Contact book.department@intechopen.com

Numbers displayed above are based on latest data collected.
For more information visit www.intechopen.com



Micromachining of Advanced Materials

Wayne N.P. Hung and Mike Corliss

Abstract

Market needs often require miniaturized products for portability, size/weight reduction while increasing product capacity. Utilizing additive manufacturing to achieve a complex and functional metallic part has attracted considerable interests in both industry and academia. However, the resulted rough surfaces and low tolerances of as-printed parts require additional steps for microstructure modification, physical and mechanical properties enhancement, and improvement of dimensional/form/surface to meet engineering specifications. Micromachining can (i) produce miniature components or microfeatures on a larger component, and (ii) enhance the quality of additively manufactured metallic components. This chapter suggests the necessary requirements for successful micromachining and cites the research studies on micromachining of metallic materials fabricated by either traditional route or additive technique. Micromachining by nontraditional techniques—e.g., ion/electron beam machining—are beyond the scope of this chapter. The chapter is organized as following: Section 1: Introduction; Section 2: Requirement for successful micromachining: cutting tools, tool coating, machine tools, tool offset measuring methods, minimum quantity lubrication, and size effect; Section 3: Effect of materials: material defects, ductile regime machining, crystalline orientation, residual stress, and microstructure; Section 4: Micromachining: research works from literature, process monitoring, and process parameters; Section 4.1: Micromilling; Section 4.2: Microdrilling; Section 4.3: Ultraprecision turning; Section 5: Summary; and References.

Keywords: micromilling, microdrilling, ultraprecision turning, minimum quantity lubrication, additive manufacturing

1. Introduction

Recent technological advancement and market need for product miniaturization demand suitable processes to mass produce three-dimensional (3D) microcomponents. Although microelectronic manufacturing techniques can produce two-dimensional (2D) microdevices using silicon and other semiconducting materials, silicon is neither robust enough for demanding engineering applications nor biocompatible for biomedical applications. Biocompatible materials and super-alloys are traditionally fabricated in bulk quantity by forging, casting, or extrusion. The recent explosion of additive manufacturing innovations has led to several revolutionary fabrication methods of engineering devices. Powder bed fusion techniques using energy beams or binding polymers to consolidate powders in

sequential layers are commonly used for metals. As in casting and welding, fabrication of a complex product by fusing re-solidified layers would introduce point, line, and volume defects in the part: dislocation entanglement, porosity, solidification shrinkage, microcrack, significant residual stress, anisotropy, rough surface finish, distortion, and undesirable microstructure are among key issues for metallic components fabricated by additively manufacturing route.

Micromachining techniques can be applied to successfully fabricate engineering components—either in meso or micro scales—from robust or biocompatible bulk materials. Micromachining is also among the key post processing techniques to enhance the quality of additively built metallic components [1–3]. This book chapter provides necessary requirements for micromachining, and cites research studies on micromachining of metallic materials fabricated by traditional or additive techniques.

2. Requirement for successful micromachining

To obtain the same surface speed as in macromachining, a machine tool must:

- a. Be capable to rotate a workpiece or tool at high rotation speeds at 25,000 rpm or above,
- b. Control spindle runout to submicron level,
- c. Have very robust mechanical and thermal structure that does not affect by vibration or thermal drift, and
- d. Have high resolution tool positioning and feeding mechanisms.

Success of micromachining depends on tool quality and precision of a machine tool. Machine spindle runout, tool concentricity and tool positioning accuracy must be in the neighborhood of 1/100 of a microtool diameter or less for successful operation. Tolerance stack up for spindle runout, tool eccentricity, and wandering of a microtool cause cyclic bending of a tool that leads to a catastrophic failure. At a low rotating speed, the displacement of a spindle can be monitored with a sensitive mechanical indicator. However, this option is not applicable for machines that operates at few thousands rpm or above. Other non-contact techniques using capacitance, magnetism, or light would be more appropriate. A laser beam can be focused on a rotating precision plug gage. The spindle displacement is then recorded on a computer for further analysis and is displayed in either frequency or time domain. Commercial laser systems can provide displacement reading to ± 10 nm resolution.

2.1 Size effect

The parameters for machining and tooling that are successfully applied in macromachining do not necessarily scale down linearly for micromachining. It is relatively easy to have a rigid turning or facing microtool, but it would require careful planning to maintain rigidity of a high aspect ratio micromill or a microdrill. Geometries of macroscale and microscale drilling/milling tools are the same: tool diameter, number of cutting flutes, point included angle for microdrill, helix angle, web thickness, clearance angle, flute length, shank diameter, and overall length. A careful selection of microtools must consider the intended machined features and

highest possible tool stiffness. The two most important geometries that affect the microtool stiffness are the tool diameter and flute length assuming the number of flutes have been chosen. It can be shown that the torsional stiffness of a mill/drill is proportional to (tool diameter)⁴ and (flute length)⁻². For a specific mill/drill tool dimension, we must adjust the milling/drilling strategy accordingly to avoid tool breakage.

If we select a drill diameter of 0.2 mm instead of 0.5 mm, then such 60% reduction of diameter will result in a reduction in torsional stiffness ΔE of:

$$\Delta E = \frac{(D_2)^4 - (D_1)^4}{(D_1)^4} = \frac{0.2^4 - 0.5^4}{0.5^4} = -97\% \quad (1)$$

Similarly, if we choose the flute length of 1.2 mm instead of 1.0 mm, this 20% change in flute length will lead to a decrease in torsional stiffness ΔE of:

$$\Delta E = \frac{(L_2)^{-2} - (L_1)^{-2}}{(L_1)^{-2}} = \frac{1.2^{-2} - 1.0^{-2}}{1.0^{-2}} = -30\% \quad (2)$$

Machining parameters that are successfully used in macromachining are not necessarily applicable for micromachining. A published literature recommends milling speed of 178 m/min and chip load of 0.1 mm/tooth for end milling 316L stainless steel using uncoated carbide tool.¹

- Macromachining: to have the said surface speed for an Ø25.4 mm end mill, the required spindle speed is:

$$N = \frac{V}{\pi D} = \frac{178 \text{ (m/min)}}{\pi(\text{rad/rev}) \times 25.4 \text{ (mm)}} \times 1000 \text{ (mm/m)} = 2230 \text{ rpm} \quad (3)$$

- Micromachining: using the same surface speed for an Ø0.1 mm micromill, the new spindle speed is:

$$N = \frac{V}{\pi D} = \frac{178 \text{ (m/min)}}{\pi(\text{rad/rev}) \times 0.1 \text{ (mm)}} \times 1000 \text{ (mm/m)} = 555,600 \text{ rpm} \quad (4)$$

A machine tool with spindle speed exceeding 500,000 rpm is rare or simply not commercially available at this time. Applying the recommended macro chip load of 0.1 mm/tooth for an Ø0.1 mm micromill would break the fragile tool since the feed/tooth is as large as the microtool diameter.

2.2 Tool sharpness

The tool edge radius is critical in micromachining. If the depth of cut (or chip load) is too shallow, the tool simply plows the material and pushes it away elastically. This elastic material layer just springs back after the tool passing. If the depth of cut (or chip load) is substantial, then a chip is formed and a new machined surface is generated. Typical fine grain carbide tools are first sintered from submicron carbide particles in a cobalt matrix, and then ground and lapped to final

¹ Machinery's Handbook, 28 ed., Industrial Press, 2008.

geometry. Optimal edge radii of 1–4 μm are typically designed for sintered tools to balance edge sharpness and edge strength. Only single crystalline diamond tools can be ground and lapped to form edge radii within nanometer range.

The threshold depth has been investigated theoretically and verified experimentally by many researchers. It varies from 5 to 40% of the tool edge radius depending on the workpiece material and original rake angles. A depth of cut (or chip load), therefore, can be conservatively set to be 50% of the tool edge radius. When machining below this threshold, a microtool just rubs the surface and deforms it elastically during the first pass. When machining with depth of cut below the critical level, the material is then being plowed at negative effective rake angle. This results in high cutting force, high specific energy, fast tool wear, rough surface finish, and significant burr [4]. In subsequent passes when the cumulative depth is above the critical depth of cut, then a tool can remove materials as chips and the cycle repeats.

It is crucial to verify the tool edge radius before deciding on cutting parameters. Measuring of tool edge radius, however, is not trivial. A tool edge radius can be estimated from a scanning electron microscopic picture when the cutting edge is parallel to the electron beam axis [5], or scanning probe microscopic picture using a probe to scan the neighborhood of a cutting edge (**Figure 1**), or by scanning the edge on an optical microscope profiler in different views to reconstruct a 3D image of an tool edge before finding its radius.

2.3 Tool materials

Having the right microtool is essential for micromachining. A microtool that successfully drills through holes on a plastic printed circuit board does not necessarily be able to drill deep blind holes on titanium alloys. Understand the requirement and select the right microtool for each condition would save time, money, and frustration.

It has been theoretically derived and experimentally proven that the smaller the chip is, then the higher the required stress will be. Microcutting tools, therefore, have to be designed for higher stress with extreme geometrical constraints. When depth of cut is smaller than the average grain size of a workpiece, each grain with different orientation generates different stress on a cutting edge and eventually fatigues the tool.

Microtools as small as 25 μm are commercially available. Common tool materials are high speed steel (HSS), cermet, carbide, cubic boron nitride (CBN),

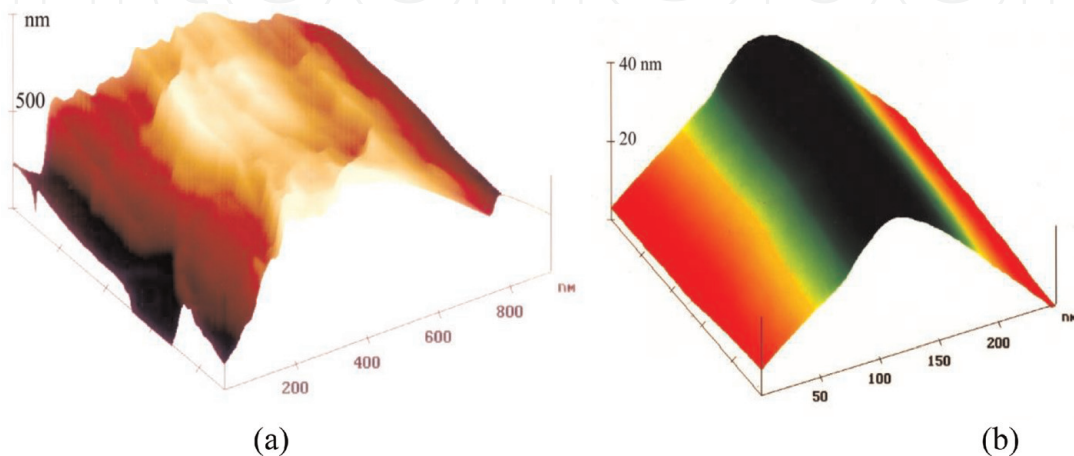


Figure 1. Tool edge radii of (a) 750 nm on a new polycrystalline diamond tool and (b) 10 nm on a new single crystalline diamond tool.

polycrystalline diamond (PCD), and single crystalline diamond (SCD). The HSS is not used in micromachining of metal since it does not have required hardness and strength to resist plastic deformation. A SCD tool is available for microturning, but not for microdrilling or micromilling. Carbide and cermet, having properties between HSS and diamond, are most suitable for microcutting tools. They are sintered from random abrasive grains in either cobalt or nickel binder with a small addition of molybdenum or chromium. A higher binder content increases the tool toughness and crack resistance, but reduces the bulk tool hardness. Having ultra-fine grain (submicron size) abrasives in a lesser amount of binder is the optimal solution since a tool with a submicron carbide grains can maintain a high hardness while improving its crack resistance against chattering, interrupted cut, or cyclic deflection due to spindle runout.

Microtool failure modes include shearing, chipping, and wear. To minimize shearing and catastrophic tool failure, a tool should be made from a high hardness substrate and its geometry would be suitable for micromachining, i.e., large included angle and sharp cutting edge. A tool with smaller than minimum included angle will be deformed and fractured in service.

Coating of microtool is still a technical challenge due to conflicting constraints for tool performance. Chemical or physical vapor deposition (CVD or PVD) techniques have been developed to coat cutting tools with mono/multiple layers of intermetallic or ceramic compounds (**Table 1**). Criteria for acceptable tool coating are numerous: uniformity of coating thickness, high hardness, high toughness, low friction, high wear resistance, surface smoothness, high chemical/diffusion resistance, and high temperature stability at a reasonable cost [6]. Although a coating thickness of 2–4 μm is acceptable for a macrotool, coating thickness on a microtool should be thinner, in the range 1–2 μm , to minimize fracture and peeling of the coating (**Figure 2**). Both CVD and PVD processes not only add the coating thickness to an edge radius, but they also increase the radius due to extra coating at a sharp corner. This is unfortunate since the thicker coating reduces the tool sharpness by enlarging the tool edge radius and causes an unfavorable plowing effect with negative effective rake angle. An uncoated microtool might perform satisfactorily, but the same machining parameter can be devastating to an over-coated microtool. Although the Calo destructive test can be used to measure coating thickness on a large object [8], it is more practical and convenient to measure coating thickness on an expensive microtool nondestructively.

Coating	Structure	Hardness (GPa)	Coefficient of friction	Coating thickness (μm)	Maximum temperature ($^{\circ}\text{C}$)
TiN	Monolayer	24	0.55	1–5	600
TiCN	Gradient	37	0.20	1–4	400
TiAlCN	Gradient	28	0.30	1–4	500
TiAlN	Multilayer	28	0.60	1–4	700
AlTiN	Gradient	38	0.70	1–3	900
ZrN	Monolayer	20	0.40	1–4	550
CrN	Monolayer	18	0.30	1–4	700
Diamond like	Gradient	20	0.15	0.5–1.5	400
AlTiN/Si ₃ N ₄	Nanocomposite	45	0.45	1–4	1200
AlCrN/Si ₃ N ₄	Nanocomposite	42	0.35	1–5	1100

Table 1.
Commercial coating for microtools.

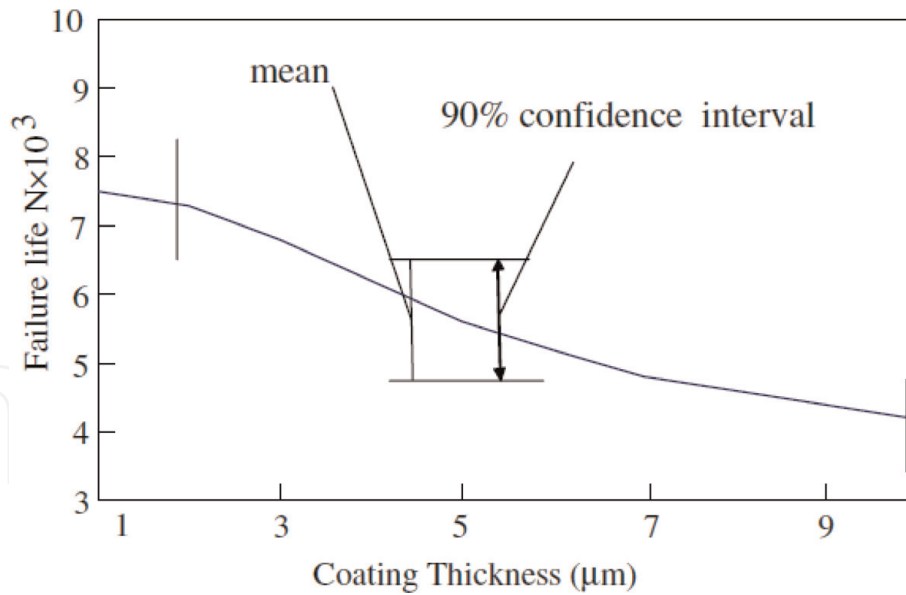


Figure 2.

Effect of tool coating thickness on tool life. TiC coated WC tool in interrupted cut [7].

Commercial instruments are available for coating thickness measurement using x-ray, magnetism, Eddy current, or ultrasound. A thin coating less than 1.5 μm following by an edge sharpening process would improve the tool performance, however, at the expense of higher tool cost. Published data indicate that micrograin carbide tools with 1.5 μm-TiN coating is the best for micromilling of H13 tool steel that has been hardened to 45 HRc.

2.4 Tool offset and positioning

Tool offset and tool positioning are crucial in micromilling and microdrilling since a high aspect ratio tool is small and extremely vulnerable. Selection of a suitable sensor for tool offsetting and tool positioning depends at least on following criteria:

- The sensor has better resolution compared to that of machine tool axis.
- The sensor should have a small working zone to cover a microtool.
- The sensor can perform at fast sampling rate for intended tool speed.

Contact techniques must be used with care for positioning a microtool. Common shop practices to find tool offsetting and positioning often damage a microtool or workpiece.

- A mechanical edge finder is adequate for most macromachining setup, but it is not suitable for micromachining especially with small and pliable part.
- Measuring resistance or current flow when a tool touching a conductive workpiece has been used with moderate success. A pulsed current might spark and damage the sharp edges of a microtool.
- An accelerometer can be mounted on either a workpiece or tool spindle housing. The difference in vibration signals indicates contact of tool and workpiece. The vibration signal, however, depends on the material of workpiece and tool, their surface roughness and detection threshold [9].

Non-contact techniques, although are generally more expensive, can provide a satisfactory accuracy and repeatability.

- Commercial laser displacement sensor with 20 μ s sampling rate (50 kHz) would be sufficient for most cases. Submicron accuracy can be achieved, but the sensor's repeatability depends on the repeatability of multiple axes of a machine tool. Both lateral and axial tool offsets have been successfully used with this technique.
- Other non-contact techniques using magnetism, capacitance, ultrasound... could be used depending on the required accuracy and the workpiece materials.

2.5 Tool damage

Tool damage can be categorized by the relative size of the damage, ranging from submicron to hundreds of microns (**Table 2**). The tool failure mechanisms include damages due to mechanical, thermal, chemical effects, or adhesion.

Mechanical effect is the most common source of tool damage. Abrasive wear is caused by low speed sliding of hard particles from workpiece or tool against the cutting tool surface (**Figure 3**). At a high cutting speed and lack of sufficient coolant/lubricant, the high temperature at tool cutting edge accelerates the tool wear due to increasing rate of diffusion and/or chemical reaction at the coating layer and the substrate below. **Figures 5a** and **5b** compare the wear of PVD coated TiAlN/TiN layer on WC tool when machining at 180 m/min; the material contrast in scanning electron microscopy highlights the faster wear rate of the coating layer when machining 3D printed titanium alloy [10].

- Attrition wear is larger than abrasion wear. This happens when one or few grains of the tool are weakened at their grain boundaries and dislodged from the tool.
- Microchipping and chipping happen when larger chunks of tool are being removed due to mechanical or thermal shocks upon loading and unloading (**Figure 4**). Machining at optimal parameters and rigid setup would reduce vibration, shock, and mechanical damage to a microtool. Chipping can occur due to high stress when machining at excessive cutting speed and feed [11]. Tool chipping also starts with microcracks due to chemical reaction among tool coating material, workpiece material, and coolant/lubricant.

Microtool damage	Damage size (μ m)	Mechanism
Abrasion	<1	Mechanical, thermal
Attrition	1–3	Mechanical, thermal
Peeling	1–3	Mechanical, chemical
Microchipping	3–10	Mechanical, adhesion
Chipping	10–30	Mechanical
Fracture	>100	Mechanical

Table 2.
Categories of tool damage.

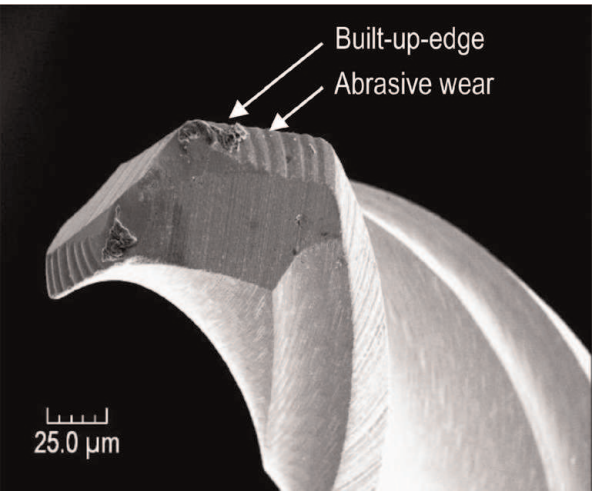


Figure 3.
Abrasive wear on a WC microdrill.

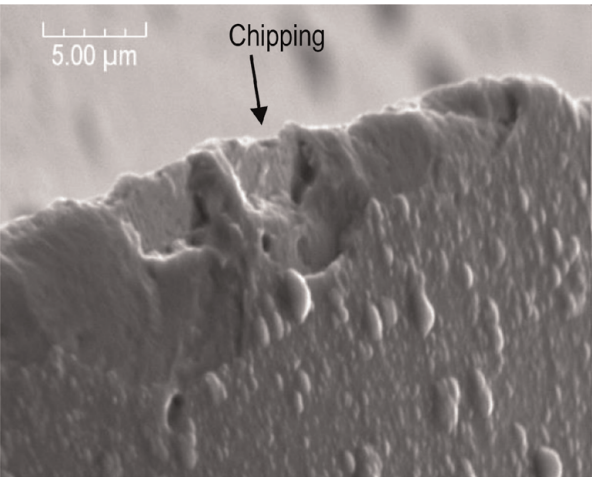


Figure 4.
Chipping of cutting edge. AlTiN coated micromilling tool.

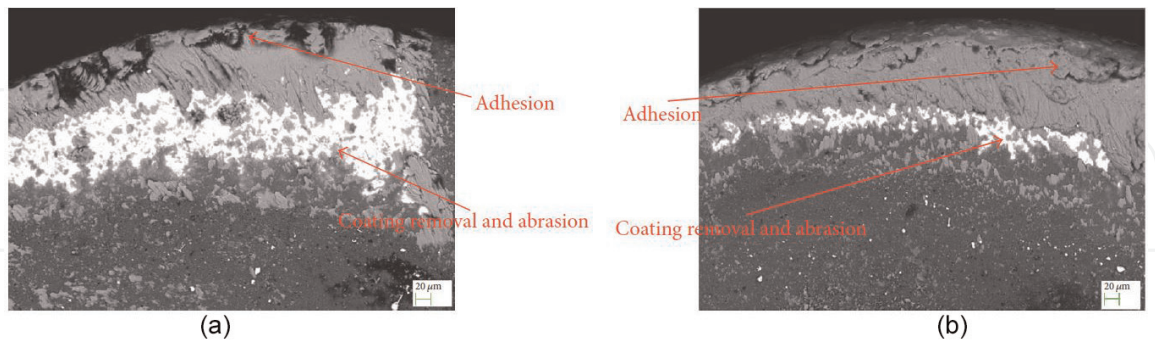


Figure 5.
Wear of coating tool after machining Ti 6Al 4V at 180 m/min on (a) wrought material and (b) selective laser melted material [10].

Thermal effect is the second cause of tool damage. A cutting tool edge is softened at high machining temperature, deformed plastically, and removed from the tool. Both high speed steel tool and carbide tool with high cobalt content are vulnerable to thermal damage. High temperature also promotes diffusion, i.e., atoms from the tool and workpiece move mutually across their interfaces, therefore degrade their properties and cause diffusion wear. Diamond with a carbon-rich matrix, or diamond-like coated tool, cannot be used with low-carbon ferrous alloy like steels or stainless steels since diamond carbonizes at temperature exceeding 600°C and

diffuses to steel due to the steel's lower carbon content and its high affinity to carbon. A tool would extend its useful life by applying proper coolant to reduce thermal damage, or having a protective coating that blocks undesirable thermal diffusion from/to a tool surface. At higher cutting speed, the thermal/diffusion wear is the main tool wear mechanism. Combination of abrasive and thermal wear can be present when both high cutting speed and material hardness are combined. After machining at a high cutting speed of 180 m/min, severe coating tool wear (**Figure 5b**) is observed after cutting the harder selective-laser-melted titanium alloy compared to that when machining the same but softer extruded material (**Figure 5a**).

Chemical damage of a tool is due to chemical reaction between tool material and its environment like air, cutting fluid, or workpiece material. Tool oxidation is common when cutting in air at high speed. An oxidation reaction is accelerated with temperature, but can be eliminated when using inert gas to shield the cutting tool from surrounding oxygen. A chain reaction can also occur and further degrade a tool. For example, iron in steel is first oxidized at high cutting temperature to form iron oxide; this iron oxide then weakens the aluminum oxide coating of a tool and leads to peeling and chipping of the coating.

Adhesion tool damage happens when a built-up-edge (BUE) welds strongly to a tool surface and then breaks away with a minute amount of tool material. Some of the BUE deposits on the back of a chip, but some can be on the machined surface thus degrading the workpiece quality (**Figure 6**). When machining soft materials, a chip tends to adhere to the tool and grows in size (**Figure 7**). When such cumulative BUE is large and becomes unstable, it is removed with chip while shearing off part of the cutting tool due to the higher adhesion strength of BUE and tool interface than the inter-grain binding strength. Stainless steel, nickel and titanium alloys are known for causing adhesion wear on carbide microtools (**Figure 8**). Adhesion damage can be reduced by using proper lubricant to reduce friction between chip and tool, by coating tool with a smooth and low friction layer, by reducing tool edge radius, or by increasing cutting speed to raise tool surface temperature and soften BUE while reducing its weldability to tool surface.

A thick tool coating, although possessing a thicker diffusion barrier, can fail prematurely due to excessive shear stress at the interface (**Figure 9**). A 5 μm thick coating is common for large carbide insert, but 1–2 μm thin coating is recommended for microtools (**Figure 2**). Failure of microtools can happen due to combination of the above mechanisms. For example, peeling of tool coating might be due to coating defects or mechanical mechanism when a large gradient of stress exists across a

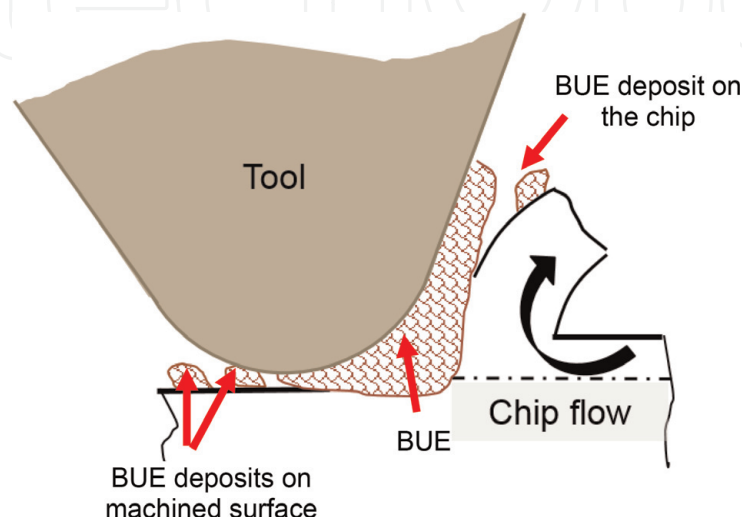


Figure 6.
Built-up-edge and its effects [12].

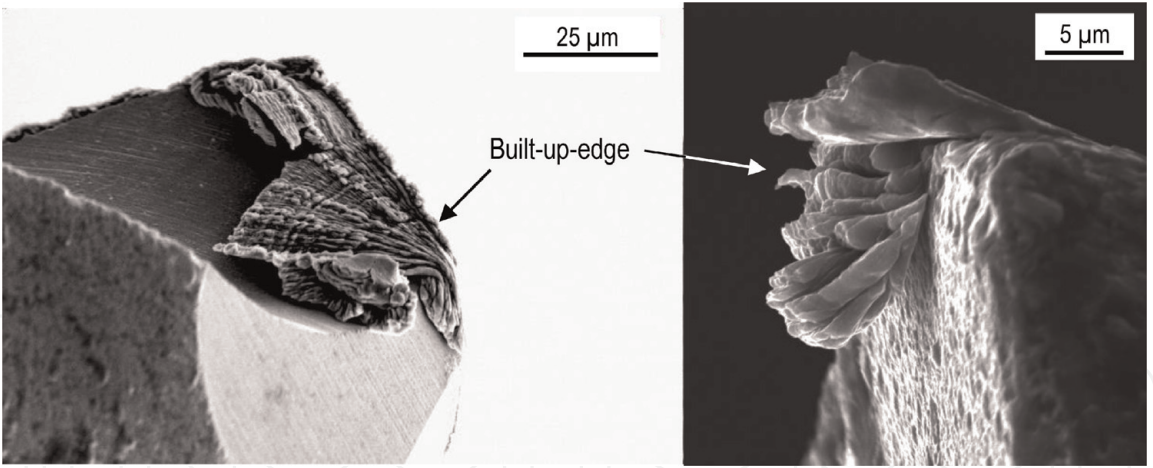


Figure 7.
Built-up-edge at the cutting edge on a microdrilling tool (left) and micromilling tool (right).

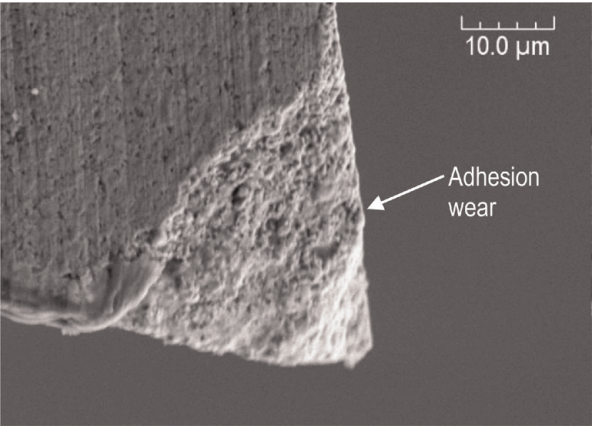


Figure 8.
Adhesion wear of a micromilling tool.

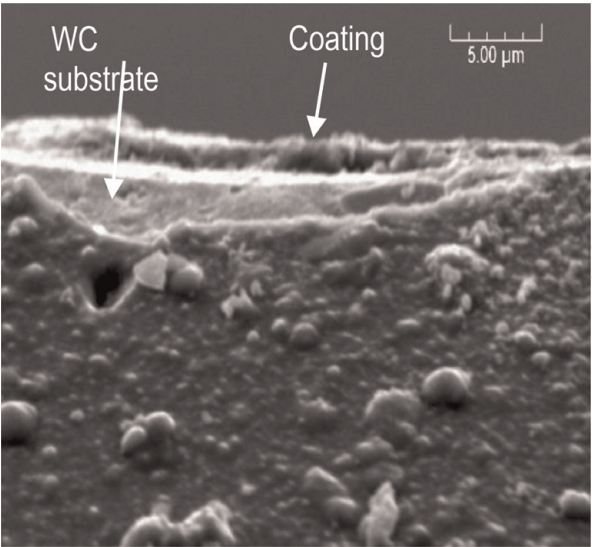


Figure 9.
Delamination of AlTiN/Si₃N₄ coating on a WC microdrilling tool.

thick coating layer; the loosen coating particles then rub and cause mechanical abrasive wear on a tool. Thermal mechanism may cause workpiece atoms to diffuse, weaken, and dislodge several tool grains as microchipping. The quenched and tempered 4140 steel fails tools by abrasion, the 304 stainless steel causes adhesion

tool wear, while the nickel supper alloy Inconel 718 damages tools by all wear mechanisms [13]

2.6 Cutting fluid

Shearing of workpiece material and relative motion between tool and chip generate a significance of heat during machining. This thermal energy could change the microstructure, plastically deform the subsurface, degrade the part quality and wear a cutting tool quickly. Cutting fluids, either oil based for lubrication or water based for cooling, should be applied appropriately for effective micromachining while evacuating tiny chips from the machined surface.

- Dry machining. Although simple, dry machining is not appropriate since it neither reduce the heat, extend tool life, nor removing chips that may interfere with machining action.
- Flood cooling. A large amount of fluid can cover a tool and workpiece, but it is not effective since the bulk liquid cannot penetrate the air boundary layer surrounding a rapidly rotate micro drilling/milling tool-typically in the range of 30,000–120,000 rpm. Increasing the flood cooling pressure, as in jet cooling, simply deflect a fragile microtool and affect the machining quality.
- Minimum quantity lubrication (MQL). A mixture of oil and compressed air is very effective for micromachining when operating at high pressure above 4 bars (400 kPa, 60 psi). The micron-sized oil droplets can be propelled at high speed to penetrate the air boundary layer, adhere to workpiece/tool zones, spread out by surface tension to effectively cool and lubricate the tool/chip interface. Correct applications of MQL extend tool life while reducing burr as reported in published literature. Advanced MQL systems include additives (lignin, nano-sized diamond particle, graphene, etc.) can further enhance the effectiveness of MQL [14].
- Cryogenic cooling. Rapid freezing of most metals at liquid nitrogen temperature (-196°C) would embrittle the materials, reduce the required energy for machining and burr formation at the expense of tool wear [15]. This expensive technique, however, requires proper insulation of tooling and fixture surrounding a workpiece.

3. Effect of materials

Micromachining is often utilized to fabricate components for miniaturized sensors, medical, optical, and electronic devices. Common engineering materials for these applications include stainless steel, aluminum, titanium, copper, and tool steel for miniature molds and dies.

Workpiece materials must meet certain conditions for successful micromachining. Unlike in macromachining, a micromachining tool is subjected to fluctuating cutting force when encounters each grain since microtool size is comparable to material grain size. A microtool is more vulnerable to fatigue fracture and the resulted surface—if the tool survives—would be rough due to different spring-back protrusion from each grain due to different crystallographic orientations of the grains, and direction-dependent properties of the material. Homogenous workpiece materials with very fine and uniform grain sizes should be chosen for

micromachining. Inclusions and large precipitates should be minimized to avoid damage to a fragile tool edge.

3.1 Ductile regime micro/nano machining

The concept of ductile-regime machining has been investigated since 1960s for amorphous brittle materials such as glasses. Silicon, germanium, and glasses have become strategic materials that are widely used to fabricate intricate components in microelectronics, optics, defense industries, and recently as micro optical-electrical-mechanical systems. Silicon and other brittle materials are known for their low machinability unless they are machined in the ductile-regime conditions. When utilized at the optimal machining conditions, only minimum effort is required for the subsequent etching, grinding, or polishing to remove the damaged subsurface. This section summarizes the theory and provides practical guidance for ductile-regime machining.

The mechanism of ductile-regime machining has been studied by many researchers. Using fracture mechanics approach, it can be shown that there is a threshold below which ductile regime prevailed:

$$d_c = \frac{\text{plastic flow energy}}{\text{fracture energy}} = A \left(\frac{E}{H} \right) \left(\frac{K_c}{H} \right)^2 \tag{5}$$

where d_c : critical depth of cut (m); A : constant. $A = 0.15$ for microscratching, $A = 0.60$ for micromachining; E : Young modulus (Pa); K_c : surface fracture toughness ($\text{Pa m}^{0.5}$); H : surface microhardness (Pa).

A shallow depth of cut, therefore, would energetically promote plastic flow rather than brittle fracture in the substrate and the chips. **Table 3** tabulates properties of some brittle materials and their experimental critical depths of cut.

The constant A in Eq. (5) varies in the range 0.1–0.6 due to measuring uncertainty of surface toughness K_c , elastic modulus E , and microhardness H in a testing environment. These properties depend on crystalline orientation of the materials, surface conditions, and tool geometry. An example of ductile regime machining on single crystal silicon wafer is shown in **Figure 10**.

- The critical resolved shear stress, on a crystalline plane due to the cutting action, is directly proportional to the Schmid factor $(\cos\lambda)(\cos\phi)$, where ϕ and λ are the orientations of the slip plane and slip direction. An ideal ductile mode machining would happen when the cutting shear stress is parallel to both the slip plane and the slip direction, otherwise a pseudo ductile mode with micro cleavages occurs. True ductile-regime machining happens only along certain crystalline orientation, but brittle machining occurs at other crystalline orientation. This explains why micromachining a crystalline specimen at the

Materials	Young modulus (GPa)	Fracture toughness (MPa m ^{0.5})	Knoop hardness (GPa)	Critical depth of cut (μm)
α-Al ₂ O ₃	275–393	3.85–5.90	19.6–20.1	1.0
SiC	382–475	2.50–3.50	24.5–25.0	0.2
Silicon	168	0.6	10	0.5

Table 3.
Properties of selected brittle materials.

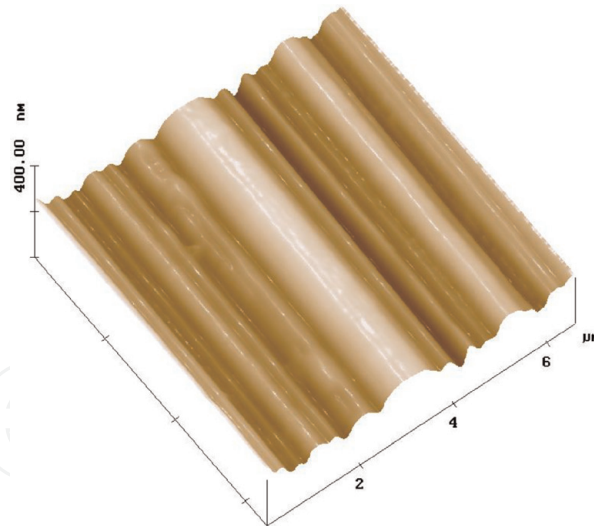


Figure 10.
Perfect ductile regime machining of (001) silicon [16].

same speed, depth of cut, and coolant produces ductile machined surfaces in one direction but brittle machined surfaces on others.

- Cutting fluid changes the surface properties of materials (K_c , E , and H) and affects conditions for ductile regime micromachining. When micromachining the (100) plane of germanium using a single crystalline diamond tool, the critical depth of cut changes from 0.13 μm with distill water as cutting fluid to 0.29 μm in dry machining.
- Tool geometry also affects the results. Plowing and fracture of material occurs when depth of cut is less than approximately half of the tool cutting edge radius. Tool with negative top rake angle is usually utilized since a negative rake causes compressive zone in the workpiece ahead and below the tool and suppresses microcrack formation.

3.2 Additively manufactured metals

The evolution of 3D printing allows metallic parts to be printed in different methods.

- Power beam fusion. Laser or electron beam are used to melt either metal wire or powder particles to form layers, then fuse these layers to form a complex shaped part.
- Material jetting. Metal powder is fed at the energy beam focused point to melt and form a part.
- Jet binding. An organic binding material is sprayed and bind metal powder in layers. The “green” part is then sintered to form the final shape.

Using any of the above techniques, an as-built part:

- i. Is warped due to high thermal induced residual stress, or non-uniform shrinkage during sintering,

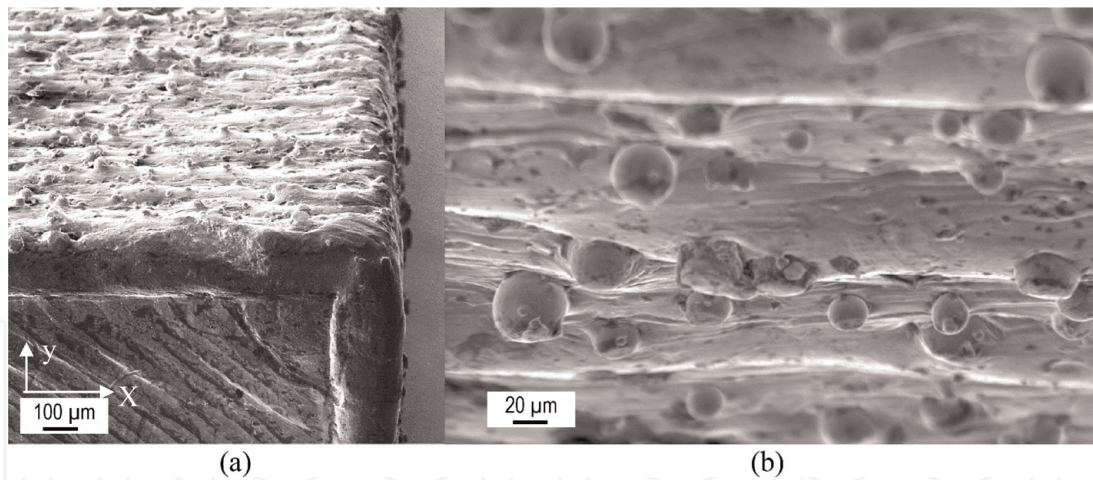


Figure 11. Surface topography of an Inconel 718 block after selective laser melting. (a) Oblique view, and (b) viewing along the building z -axis.

- ii. Has very rough surface (typically 15–20 $\mu\text{m Ra}$), and
- iii. Is filled with surface defects (e.g., microcrack, shrinkage cavity, partially welded powder particles, etc.) as shown in **Figure 11**, and volume defects (e.g., porosity, inclusion, shrinkage cavity, etc.).

Post processing of the as-built metal parts must be performed so that they can meet required engineering criteria for surface finish or dimensional/form tolerances. Micromachining is the most effective post processing technique to control the surface and dimension of local areas of additively manufactured metals due to its high removal rate and well-established computer numerical controlled (CNC) industry.

4. Micromachining

Micromachining refers to removal of material subtractively in micron scale. The process can be done by (i) conventional processes, i.e., removing material mechanically with hard tools in contact with a workpiece and removing minute amount of material as chips, or (ii) non-conventional processes, i.e., removing material by other physical mechanisms such as optical, thermal, chemical, electrical, or combinations of these. The following section focuses only on the three major conventional techniques, namely micromilling, microdrilling, and microturning of advanced materials.

4.1 Micromilling

Micromilling is among the most versatile microfabrication processes. Although alternative nontraditional processes to produce microfeatures (e.g., laser micromachining, electrical discharge micromachining, electrochemical micromachining, chemical microetching, electron/ion beam micromachining) are available, these processes are either cost prohibitive, or inferior when comparing resulted surface and subsurface integrity, anisotropic aspect ratio, material removal rate, or feature quality. Successful micromilling requires new tool geometry, tool material, machining parameters, and machining skills. It is technically incorrect and

costly to perform micromilling by just scaling down a milling cutter, or parameters from macroscale milling.

Tool material. Carbide tools should be sintered from fine grains, and precisely ground to obtain a micron-level cutting edge radius.

Milling direction. Down milling is the preferred mode since a micromill will engages a workpiece and removes a wedge shape chip with decreasing chip thickness. In contrast, a tool in up milling would rub on the workpiece until the effective chip thickness is greater than 0.5 cutting edge radius. Down milling also produces less amount of burr.

Lubrication. Minimum quantity lubrication should be used with all micromachining. A nozzle should be as closed as possible and is positioned to let the cutting flute pulls the mist into the cutting zone. Tool and workpiece should be arranged to avoid stagnant zone, or being blocked or interfered by chips [17].

Tool vibration. Avoid unnecessary disengaging then engaging of microtool and workpiece in a milling program. Vibration and bending of a microtool at starting and ending could fatigue and shorten tool life of a microtool (**Figure 12**).

Commercial micromills are available for diameter of 25 μm and above. Optional geometries include:

- Flute lengths: standard or extended length (10–80% longer)
- Number of flutes: 2, 3, or 4
- Helix angles: 25°, 30°, 50°
- End configuration: hemisphere or flat.

As mentioned above, the BUEs on a cutting tool surface can break and deposit on a machined surface as shown in **Figure 13**. Measuring area surface finish S_a would combine the roughness contributed from milling parameters (e.g., speed, feed), tool and machine condition (e.g., vibration), and surface irregularities (e.g., pore and BUE). The BUEs is reduced when an optimal condition of MQL is used, low chip load, and higher speed. In a study of micromilling 316L stainless steel, the amount of BUE is significantly diminished when cutting at speed higher than

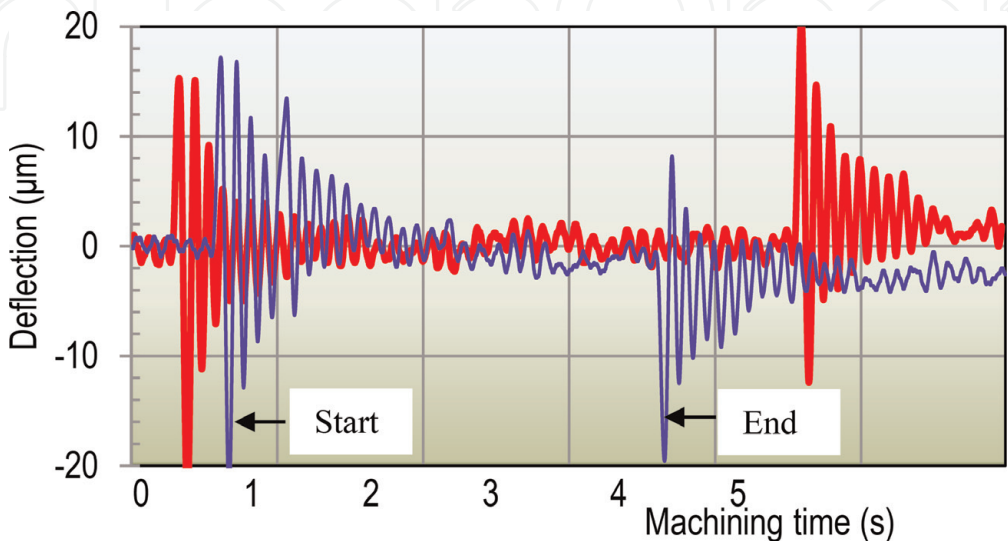


Figure 12.
Vibration of a micromill when engaging and disengaging a workpiece. Carbide mill $\varnothing 1\text{ mm}$, 316L stainless steel, 25,000 rpm, 10 $\mu\text{m}/\text{tooth}$ feed, 0.348 mm axial depth, 0.558 mm radial depth.

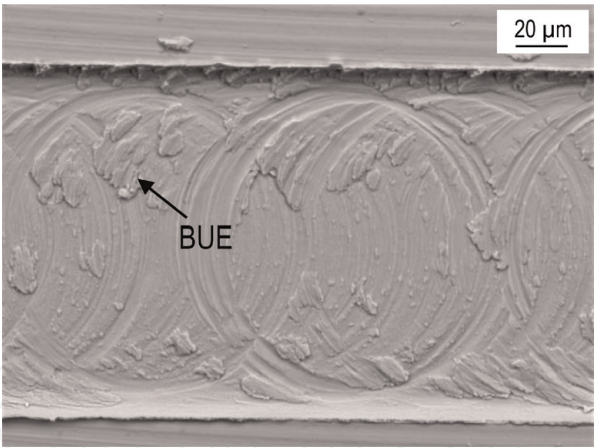


Figure 13. Built-up-edges deposit on machined Ti 6Al 4V surface. Micromilling at 9.6 m/min, 0.1 μm/tooth, 10 μm axial depth. Dry [18].

30 m/min (**Figure 14**). Perhaps the high temperature at high cutting speed improves the material plasticity and reduces the weldability of BUEs on cutting tool tip.

Lack of BUEs on coated tool also results in better surface finish of micromilled channels on 304/316L stainless steels, NiTi alloy, A36 low carbon steel, 6061-T6 aluminum, and Ti-6Al-4V titanium alloy. The AlTiN coating effectively increases tool life while reducing burrs significantly when micromilling 304 stainless steel. The incompatibility of the coating on specific material workpiece prevent BUE formation, therefore, shear the materials as chips rather than deforming it as burr (**Figure 15b**). The effect of micromilling mode is also shown when up-milling tends to generate more burr than down-milling (**Figure 15a**).

The theoretical surface finish of machined surface after milling with a flat-end tool can be shown to be:

$$R_a = \frac{5}{18} f_t \tan \alpha \tag{6}$$

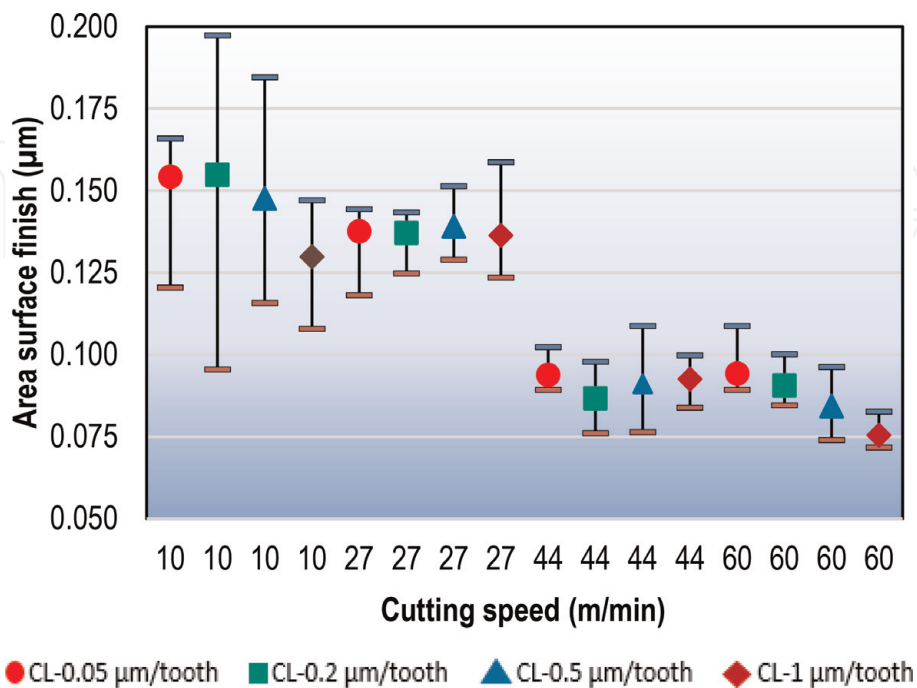


Figure 14. Effect of cutting speed and chip load on area surface roughness S_a . Each range plot shows the maximum, minimum, and average of 15 measurements. Micromilling 316L stainless steel [12].

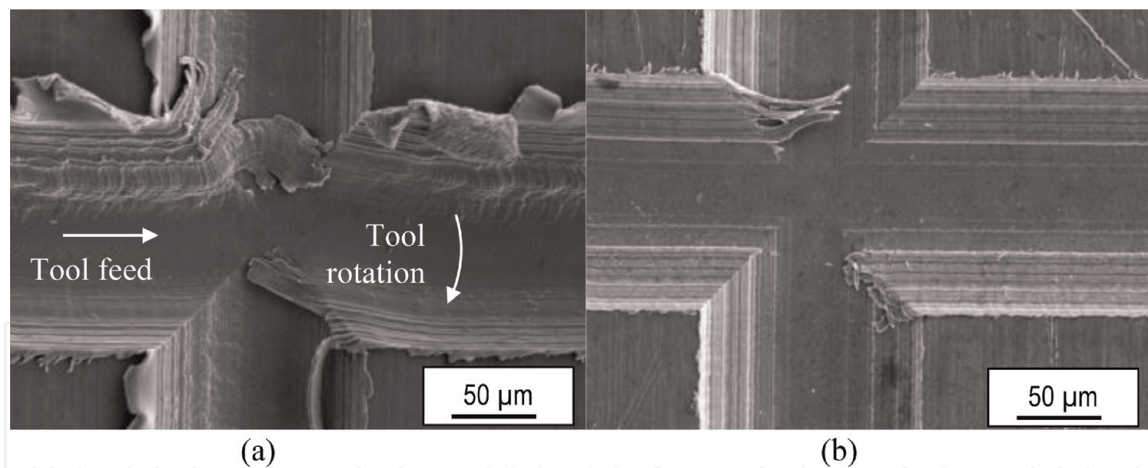


Figure 15. Effect of tool coating on resulting burrs: (a) uncoated $\phi 152 \mu\text{m}$ tool, milling 304 stainless steel, 24 m/min, 0.1 $\mu\text{m}/\text{tooth}$, MQL; and (b) AlTiN coated $\phi 198 \mu\text{m}$ tool, milling 304 stainless steel, 24 m/min, 0.1 $\mu\text{m}/\text{tooth}$, MQL [19].

And that for a ball-end milling tool is:

$$R_a = 0.2423 \frac{f_t^2}{D}. \quad (7)$$

Rearranging Eq. (7) to have:

$$D \cdot R_a = 0.2423 f_t^2 \quad (8)$$

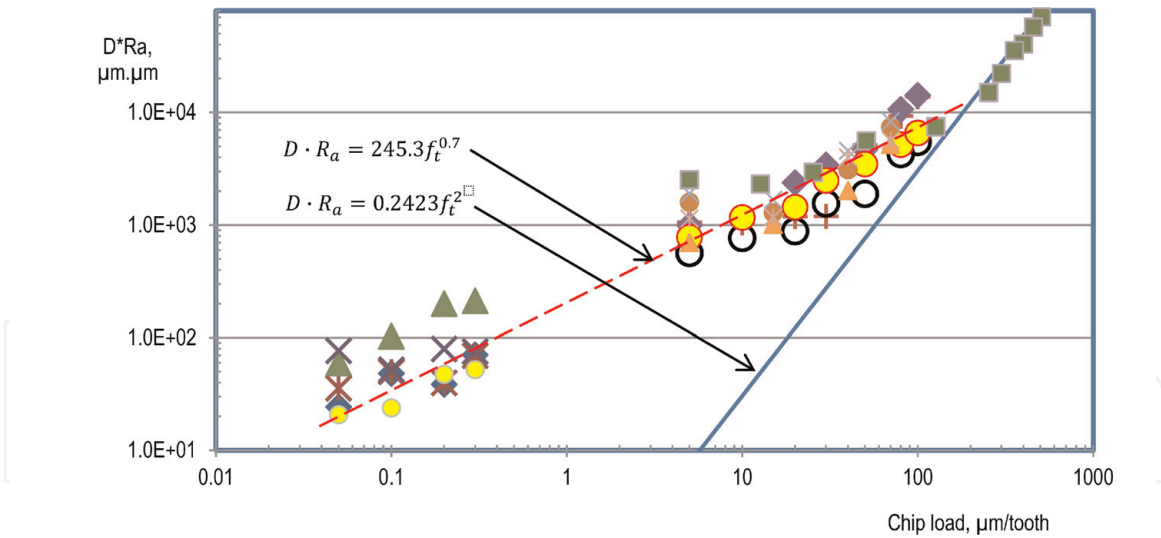
where R_a : average surface finish (μm); f_t : chip load ($\mu\text{m}/\text{tooth}$); D : diameter of ball-end milling tool (μm); α : concavity angle, or end-cutting-edge angle ($^\circ$).

Both Eqs. (6) and (8) predict the dependent of chip load on surface finish R_a . When plotting Eq. (8) using experimental data from different tool diameters and different chip loads, then Eq. (8) is confirmed with data in macromilling when chip load $>100 \mu\text{m}$ but not with smaller chip load for micromilling (**Figure 16**). The reason for a higher surface finish is the intermittent BUEs, although small, smear and degrade the machined surface.

Similar experimental results is shown in **Figure 17** for micromilling of additively manufactured Ti 6Al 4V alloys. At a very low chip load of 0.1 $\mu\text{m}/\text{tooth}$, the presence of significant BUEs on machined surface degrades the surface quality as indicated by high surface roughness R_a . The surface improves at higher chip loads, by reduction of BUEs, but is gradually increased with chip load as predicted by Eq. (6). Similar surface roughness result was reported for machining 7075 aluminum alloy [21].

Post processing by micromachining of additively manufactured metals have been investigated. Few studies have compared machinability of selected metals produced by conventional route (e.g., casting, extrusion, rolling, etc.) and by additive manufacturing route (e.g., powder bed fusion, direct energy deposition, etc.). Limited machining investigations on Inconel 625, Inconel 718, Ti 6Al 4V, H13 tool steel, Ti 48Al 2Nb 2Cr alloy, 17Cr 4Ni stainless steel, and 316L stainless steel have concluded that the AM metals in general have lower machinability compared to the conventional metals.

Machinability is affected by microstructural changes in a material. A quick comparison between the microstructure of extruded and SLM'ed Inconel 718 shows the contrast of the same materials after different manufacturing routes. Uniform



- ◆ Center of the slot; uncoated tool d0.152mm; V=24m/min; Ap=0.03mm; after 12mm of 304 SS
- ✕ Center of the slot; coated tool d0.198 mm; V=24m/min; Ap=0.03mm; after 12 mm of 304 SS
- ▲ Center of the slot; uncoated tool d0.152mm; V=24m/min; Ap=0.03mm; after 12mm of 304 SS and 12mm of 316L SS
- ✕ Center of the slot; coated tool d0.198mm; V=24m/min; Ap=0.03mm; after 12mm of 304 SS and 12mm of 316L SS
- ✚ Center of the slot; uncoated tool d3.175mm; V=60m/min; Ap=0.1mm; after 10mm of 6061-T6
- Side wall of the slot; uncoated tool d3.175mm; V=60m/min; Ap=0.1mm; after 10mm of 6061-T6
- ◆ Center of the slot; coated tool d3.175mm; V=60m/min; Ap=0.1mm; after 10mm of 6061-T6
- Side wall of the slot; coated tool d3.175mm; V=60m/min; Ap=0.1mm; after 10mm of 6061-T6
- Center of the slot; uncoated tool d3.175mm; V=30m/min; Ap=0.05mm; after 20 mm of A36 low carbon steel
- ▲ Side wall of the slot; uncoated tool d3.175mm; V=30m/min; Ap=0.05mm; after 20 mm of A36 low carbon steel
- ✕ Center of the slot; coated tool d3.175mm; V=30m/min; Ap=0.05mm; after 20 mm of A36 low carbon steel
- ✕ Side wall of the slot; coated tool d3.175mm; V=30m/min; Ap=0.05mm; after 20 mm of A36 low carbon steel
- Center of the slot; coated tool d0.198mm; V=24m/min; Ap=0.03mm; after 12mm of 304 SS, 12mm of 316L SS, and 8mm of NiTi
- Center of the slot; uncoated tool d9.525mm; V=15m/min; Ap=0.3mm; 6061-T6

Figure 16.

Average surface finish at center of milled microchannels. Ball-end milling tools $\phi 152-9525 \mu\text{m}$, workpiece materials 6061-T6, A36 steel, NiTi, 304/316L stainless steels, in MQL condition [19].

microstructure of the extruded specimen is expected (**Figure 18**). The mechanical properties of extruded specimen could be slightly different in longitudinal and transversal directions due to preferred grain orientation along the extrusion direction. In contrast, the fast heating and cooling rate of SLM'ed Inconel 718 creates alternate layers along the laser paths and hard particles in the microstructure (**Figure 19**). The obvious changes in microstructure result in different mechanical properties, therefore, affecting machinability. Fast cooling in SLM'ed Inconel 718 also forms brittle Laves particles and traps pores near an edge (**Figure 20a**). During machining, some particles are broken, smeared along the tool path and probably chipped the cutting tool. Porosity is unavoidable in AM metals. The burr on top of those micron-size pores after micromachining is difficult to remove mechanically (**Figure 20b**). Although hot isostatic pressing (HIPping) can eliminate porosity, some materials (e.g., Inconel 718) are aged at HIPping temperature; the resulted precipitates increase the material strength but reduce its machinability (**Figure 21**).

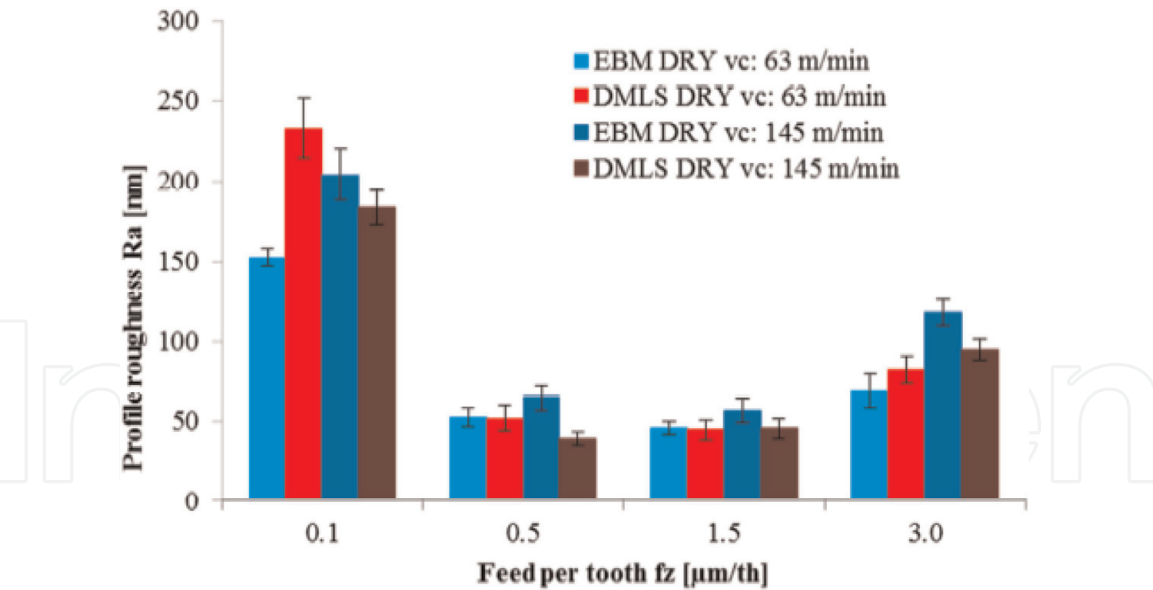


Figure 17.
Effect of chip load and cutting speed on surface finish. Micromilling of Ti 6Al 4V fabricated by electron beam melting, and direct metal laser sintering [20].

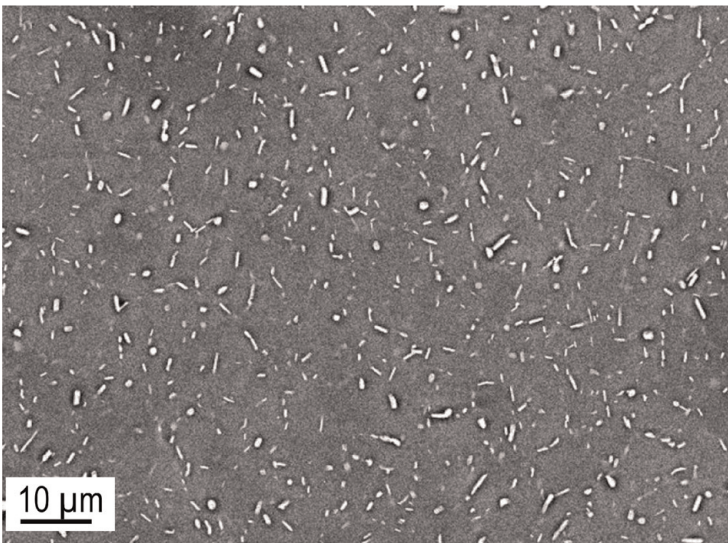


Figure 18.
Uniform microstructure of extruded Inconel 718. Viewing along the extruding direction.

Conflicting literature data are probably due to different process parameters for AM metals and different scanning strategies. For example, the precipitation hardenable 17Cr 4Ni stainless steel was reported to have near fully martensitic structure and high yield strength than the cast alloy, but the opposite conclusion was found in another study.

Advanced cutting fluids and techniques have been applied for micromilling of advanced materials. Poor results are reported when using a pressurized jet to flood cool during micromilling of Ti 6Al 4V. The fragile tool (200 μm diameter, AlTiN coated, 1.25 $\mu\text{m}/\text{tooth}$ feed, 30,000 rpm rotating speed, 20 μm depth of cut) being deflected and vibrated under pressurized jet, generates large burr and rough surface (**Figure 22a**), while cutting a large slot width (**Figure 22b**). Applying MQL with flow in the feeding direction solves these problems. When using MQL at high air pressure above 5.5 bar, a nozzle with rough internal surface breaks the lubricant into smaller droplets and effectively improves tool life of micromilling tools [24].

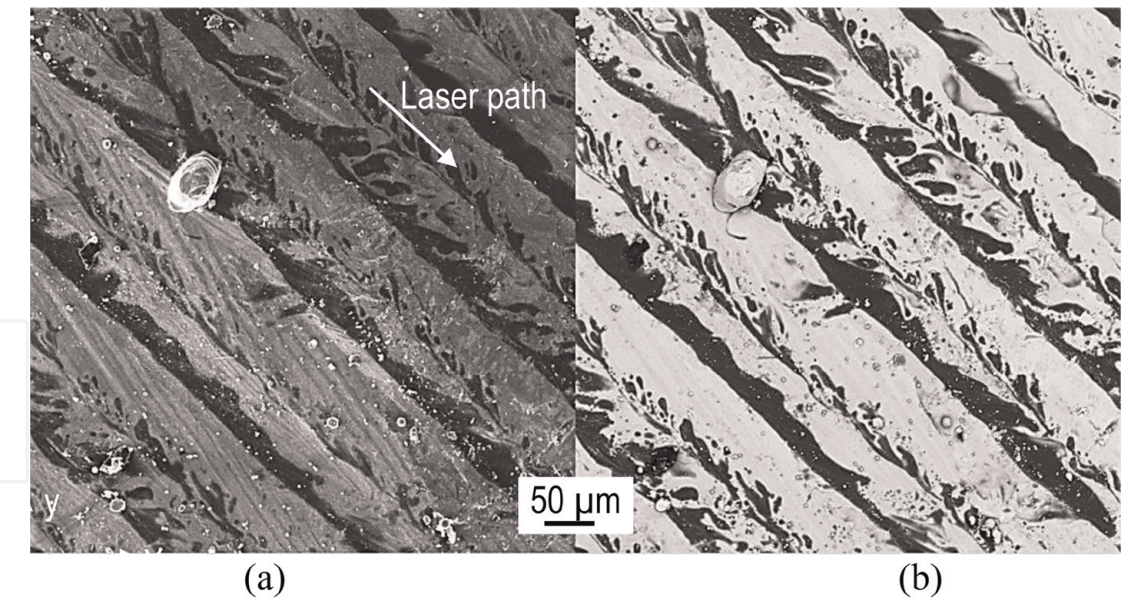


Figure 19. Microstructure of SLM'ed Inconel 718 by scanning electron microscopy in (a) secondary electron mode, and (b) back scattered electron mode. Notice the different layers across the laser scanning paths.

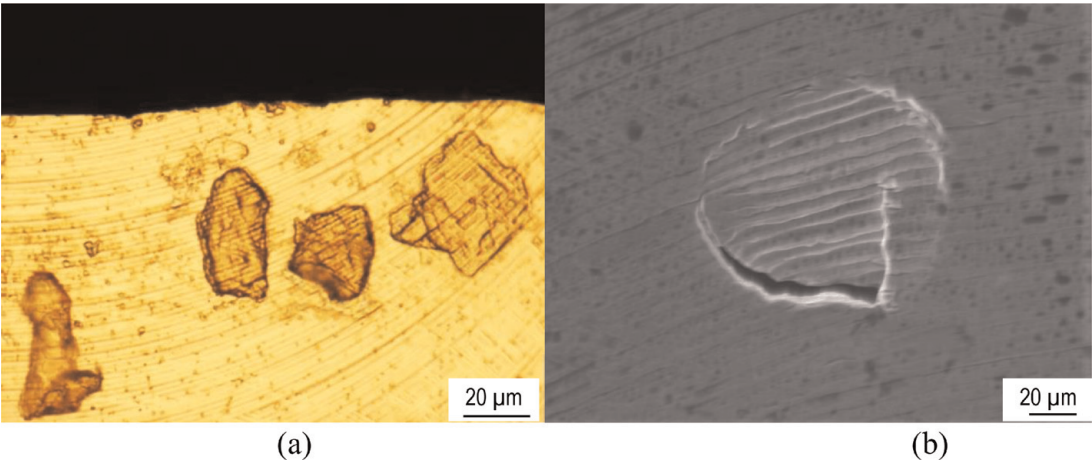


Figure 20. Irregularities in selective laser Inconel 718. (a) Sheared Laves particles after micromilling, (b) A machined micropore with burr.

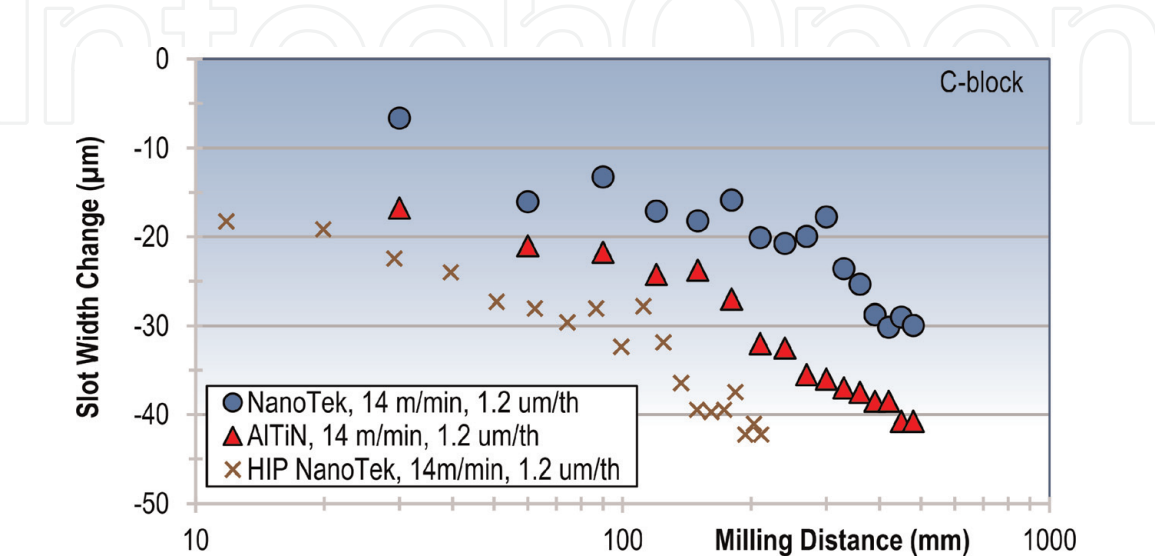


Figure 21. Micromilling of SLM'ed Inconel 718. Change of slot width with milling distance. Minimum quantity lubrication, 50 μm depth of cut [22].

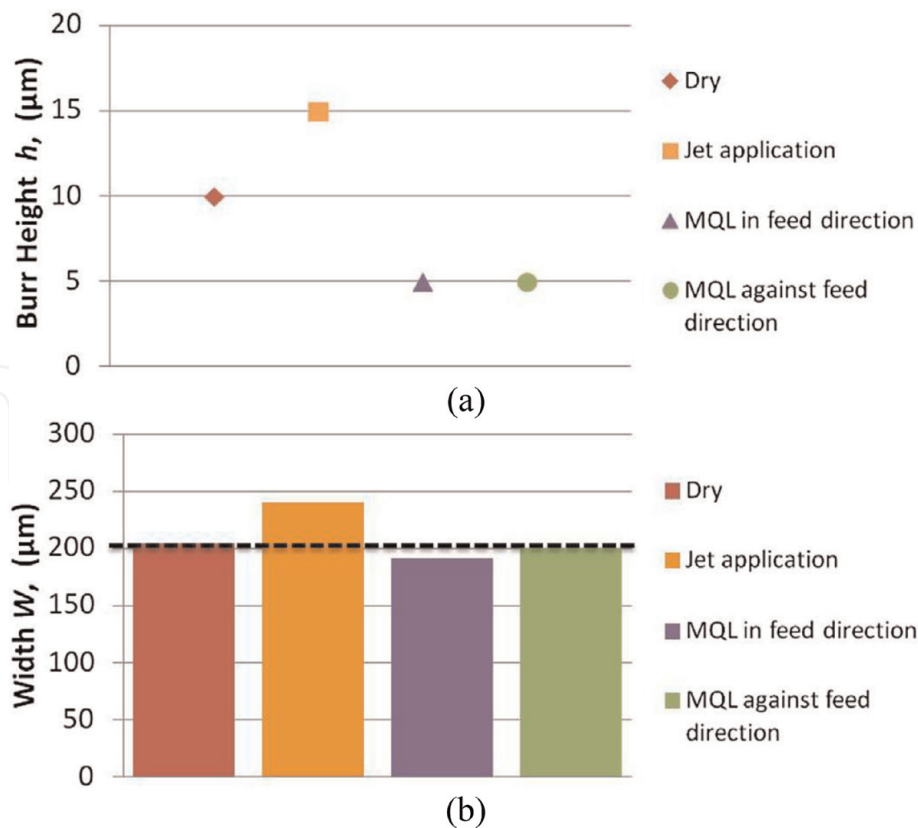


Figure 22.
Effect if different cooling methods on (a) burr formation, and (b) resulted slot width. Micromilling of Ti 6Al 4V [23].

Effort was made to produce an environmentally friendly cutting fluid while enhancing the cutting fluid performance. Lignin is a biodegradable product from wood. It can be mixed in alcohol then TRIM water soluble as cutting fluid. Micromilling tests are performed with 396 μm diameter milling tool on 6061 aluminum and 1018 steel. The optimal concentration of 0.015% lignin seems to provide the best lubricating and cooling effects when reducing the cutting forces on both materials (**Figure 23**).

Cryogenic precooling can be used to reduce BUE formation and its effect on part quality. Liquid nitrogen, dispensed in front of a microtool in a micromilling test on Inconel 718. The tool (760 μm diameter, AlCrN coated) is used at 48 m/min speed, 1.25–5 $\mu\text{m}/\text{flute}$ chip load, 0.1–0.2 mm depth of cut for a constant distance of 120 mm. The cryogenic condition embrittles the Inconel material so it can be micromilled in brittle mode with minimum plastically deformed burr and BUEs. The result is the low surface roughness at different chip loads (**Figure 24a**) and depth of cuts (**Figure 24b**). However, the brittle chip debris are abundant and might interfere with subsequent machining passes. No chip debris is seen when MQL is used.

The positive results of cryogenic cooling on Inconel 718, however, was not confirmed in a similar study on micromilling of electron beam melted Ti 6Al 4V. The 300 μm cutting tools were utilized at 63–145 m/min speed, 0.1–3.0 $\mu\text{m}/\text{tooth}$ chip load, and 30 μm axial depth of cut. The temperature of the workpiece was at $-155 \pm 5^\circ\text{C}$ with liquid nitrogen. No brittle chip debris are seen, ductile burr are visible (**Figure 25a**), and the surface profile (R_a finish) are similar for dry, MQL, and cryogenic conditions. The machined surface is work-hardened after micromilling at cryogenic condition as shown in the nanohardness results below the surface (**Figure 25b**). This implies the material is not truly embrittled as planned.

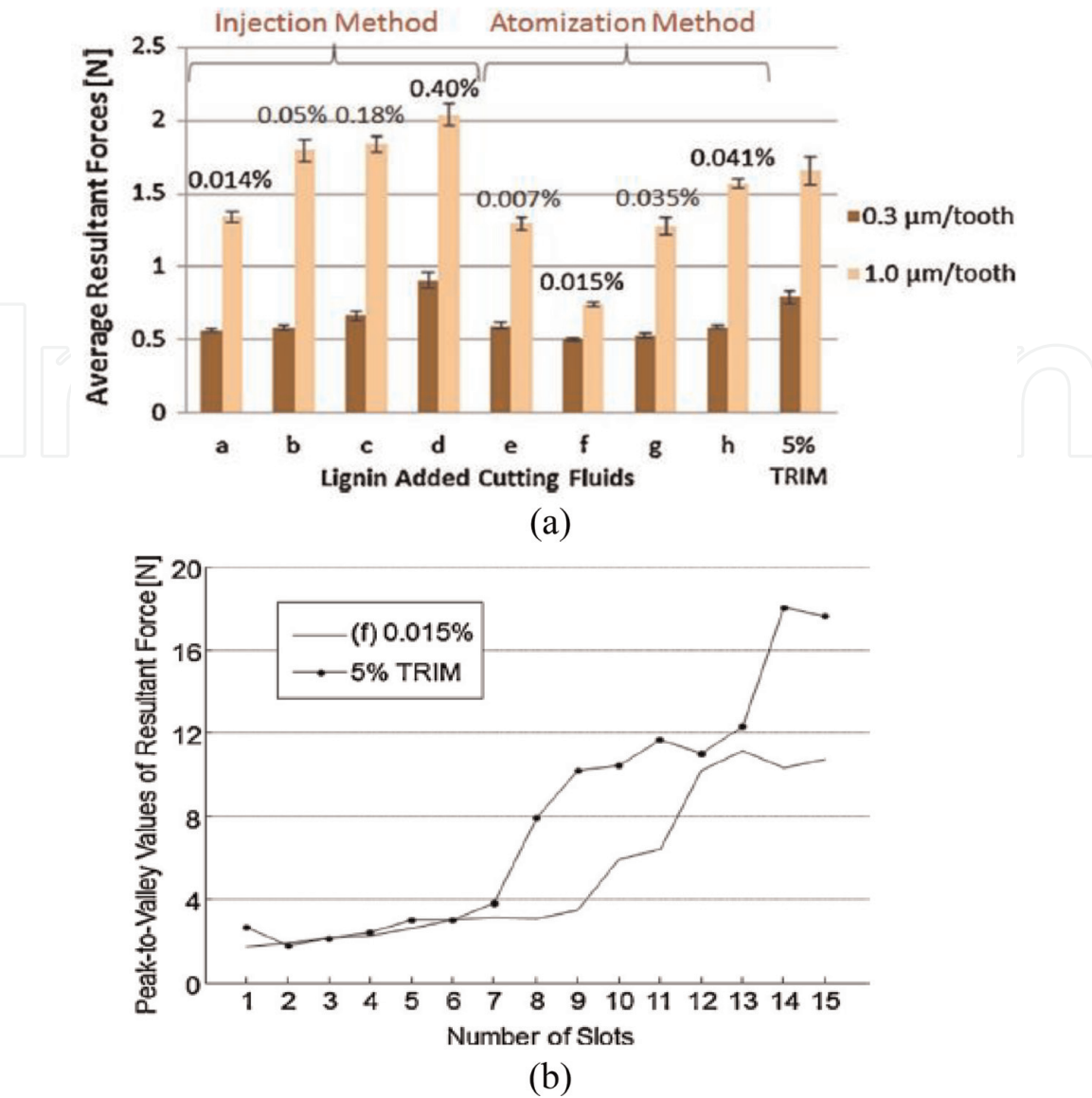


Figure 23. Effect of atomized cutting fluid with lignin on micromilling of (a) 6061 aluminum and (b) 1018 steel [25].

Another effective additive in MQL is nano-sized diamond particles. This application, applied to microdrilling, will be presented in the next section.

4.2 Microdrilling

Microdrilling is a more complex operation comparing to turning or milling. Chip removal and effectively supplying of cutting fluid are easy with the latter, but not with microdrilling due to extremely limited space around a microdrill.

Tool material. As with a micromill, a carbide microdrill should be sintered from fine grains, and ground to small cutting edge radius.

Hole quality. Spindle runout, tool eccentricity, and wandering of a microdrill cause cyclic bending of a tool and could lead to a catastrophic failure. To control drill wandering, precision pre-drilling of a center hole can be tried, or the workpiece surface must be ground to minimize deflection of a slender drill when starting on an irregular surface.

Micromist with fixed nozzle pointing to the drill tip and making an angle of 60–70° with the tool axis is recommended. This way, the chip is blown away after each pecking cycle and the microdrill is re-lubricated before re-entering into the hole.

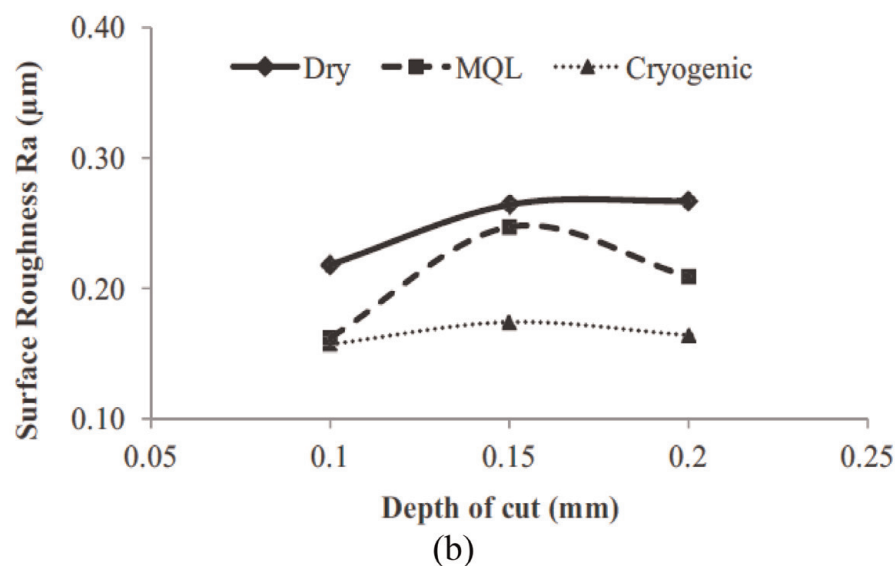
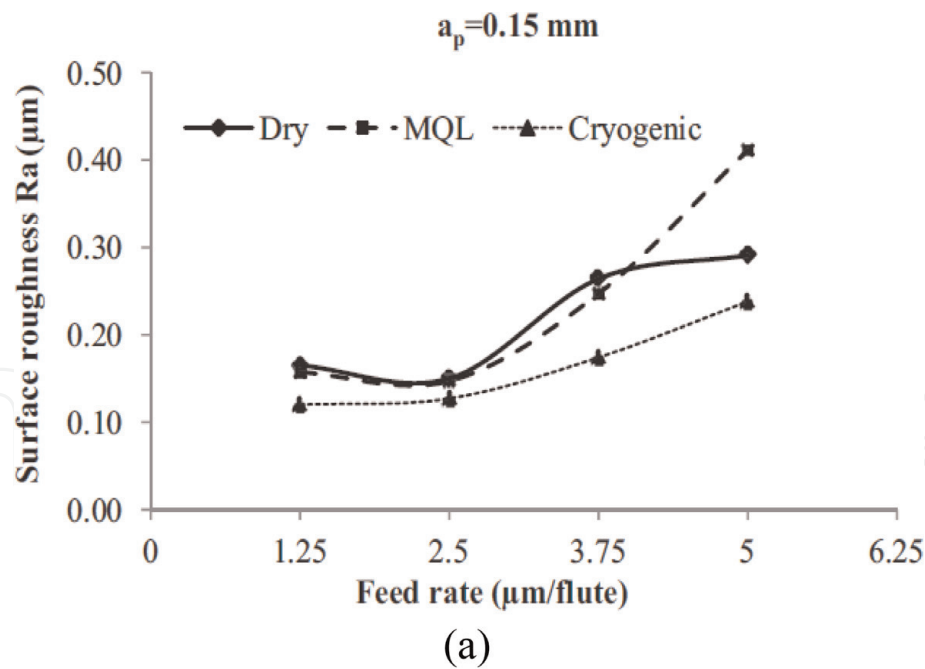


Figure 24.
Effect of different cooling strategies on micromilling of Inconel 718 (a) effect of chip loads, and (b) effect of axial cutting depth (Ucun, 2014).

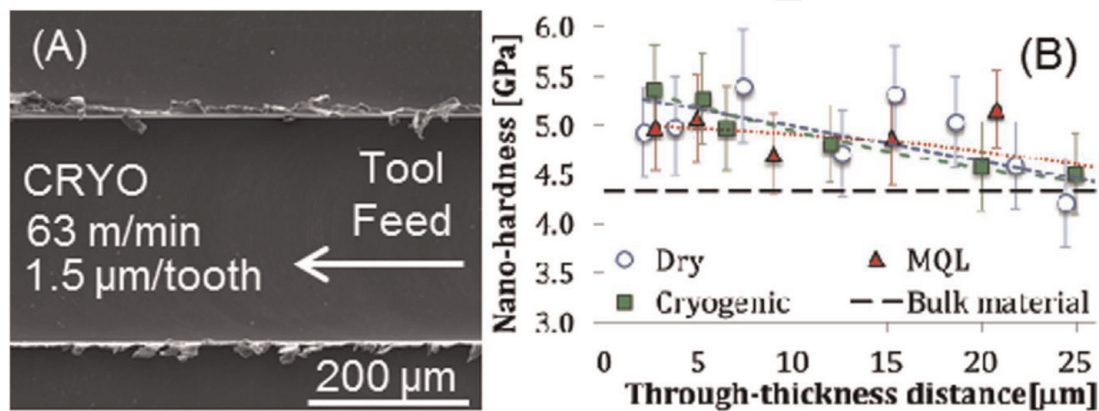


Figure 25.
Effect of cryogenic cooling on micromilling of electron beam melted Ti 6Al 4V [26].

High aspect ratio. Pecking is essential for microhole drilling since chips have to be extracted and cutting fluid must penetrate into a small and deep microhole. The pecking depth can be substantial in the beginning, but it must be gradually reduced when drilling at deeper depths. One can start with an initial pecking depth of (2*drill diameter) and gradually reduce it to (0.5*diameter) at the hole depth of (10*diameter). It is convenient to program pecking cycles in microdrilling following the equations below.

$$\frac{P}{D} = \frac{1}{9}(-1.5R + 19.5) \quad \text{for } R \leq 10 \quad (9)$$

$$\frac{P}{D} = 0.5 \quad \text{for } R > 10 \quad (10)$$

where P : incremental pecking depth (mm); D : drill diameter (mm); R : progressive drill aspect ratio = current hole depth/drill diameter.

Although application of MQL in micromachining is necessary, other researchers have found ways to improve its effectiveness. Nanoparticles are mixed in MQL oil to improve its performance in microdrilling. The nano-sized particles of CNT-C60, TiO_2 , Al_2O_3 , MoS_2 , and diamond would increase the thermal conductivity of the fluid thus prolong the tool life while reducing burr. In an experimental microdrilling study, uncoated microdrills of 100–500 μm diameters are used at 10–15 mm/min, 30,000–60,000 rpm spindle speeds, while varying the concentration of 30 nm diamond particles in the range 0–4%. The MQL system is used at 3-bar air pressure to drill a constant 0.3 mm depth. The optimal conditions for low torque and thrust force are experimentally obtained to be 60,000 rpm and 2% concentration.

Inspection of a microdrilled and tapped hole would be difficult. Destructive technique by sectioning a part is time consuming, expensive, and error prone since the internal features might be distorted by releasing of residual stress. X-ray computed tomography (CT) has been utilized to evaluate drilled and tapped Ti 6Al 4V dental implant fabricated by direct metal laser sintering. The best microdrilled hole quality—cylindricity and perpendicularity—is achieved at the lowest testing drill speed of 60 m/min and the lowest chip load of 10 $\mu\text{m}/\text{flute}$. **Figure 26a** shows the sectional view of the CT image of a drilled and tapped dental implant. Detailed observation and measurement can then be performed (**Figure 26b**).

Finite element modeling of a microdrill was done to find the limiting drilling parameters that would fracture a microdrill catastrophically. It was assumed that

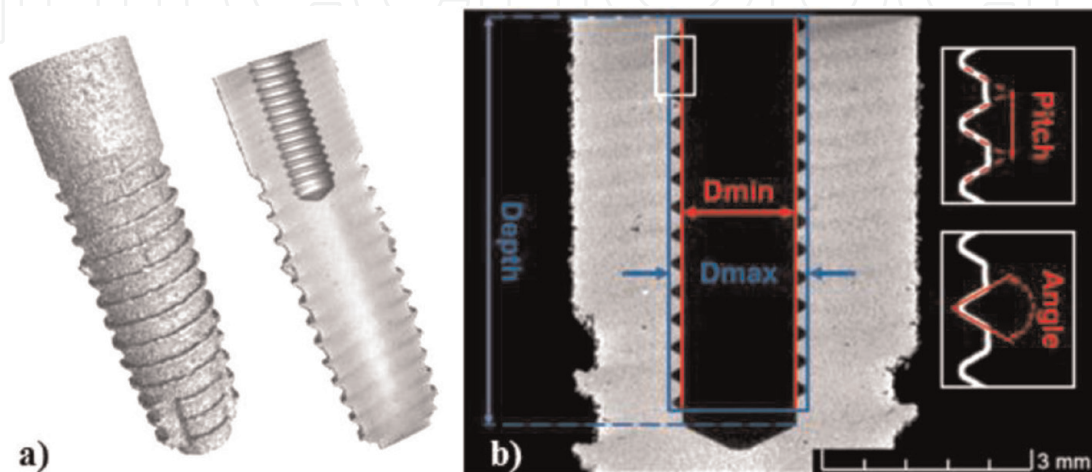


Figure 26. Inspection of drilled and tapped microhole by X-ray computed tomography. Ti 6Al 4V dental implants fabricated by direct metal laser sintering [27].

the drill shank is rigid, axial thrust force and torsional torque can fail a drill in either buckling mode or torsional mode. Transverse shear strength in three-point bending test of a sintered carbide tool is estimated to be half of the material tensile strength. This study used commercially pure (CP) titanium, 316L stainless steel, 6061-T6 aluminum, PEEK plastic, and Nitinol (51 wt% Ni 49% Ti) shape memory alloy. Some surfaces were faced milled on a milling machine, others were milled, hand ground and then finish polished with 1 μm diamond paste. Microdrilling was performed with $\varnothing 100\text{--}150\text{ }\mu\text{m}$ drill diameter, 135° point angle, 30° rake angle, $40\text{--}44^\circ$ helix angle, 2 flutes, and 1.50–3.50 mm flute length. Some were coated with AlTiN or AlTiN/Si₃N₄ under the trade name Nanotek.

The classical Taylor's equation has been applied for macromachining, micromachining, and is used for microdrilling to show the effects of chip load and tool coating. For the same cutting speed of 20 m/min and comparable drilling distance of about 35 mm, the CP titanium can be microdrilled 400% faster than 316L stainless steel since the chip load for the former is 0.1 μm and that for the latter is 0.02 μm . Also, AlTiN coated drills improve tool life by at least 122%. This drilling operation is stopped after drilling all possible holes on the test blocks (Figures 27 and 28). Negligible tool wear are observed when drilling 6061-T6 aluminum and PEEK plastic, therefore, no modeling is necessary.

Burr, hole size, hole position, and work hardening around a drilled hole contribute to the hole quality. During the initial engagement of drill and workpiece surface, a slight lateral motion of the drill chisel edge is sufficient to bend and misguide the slender microdrill. Drill wandering refers to the deviation of a drilled hole from its intended position. A machined surface is rough enough to cause wandering of microdrills. A sloped ridge on a rough surface bends and deviates the drill axis from intended position. Such deviation causes drill wandering, significant burrs, and irregular hole diameters. The hole quality is improved significantly when drilling on a polished surface at the same or more aggressive drilling parameters. An improvement of 27% in hole center deviation is achieved for the polished surface of CP titanium (Figure 29). Similarly, an improvement of 260% on hole deviation is achieved when drilling a polished PEEK block.

Vickers microhardness near a drilled surface is obtained to study the level of plastic deformation and work hardening below a drilled surface. The hardness near the drilled surface is found to be 15% higher than those at the unmachined zone (Figure 30). The work hardening effect is caused by plastic deformation of the

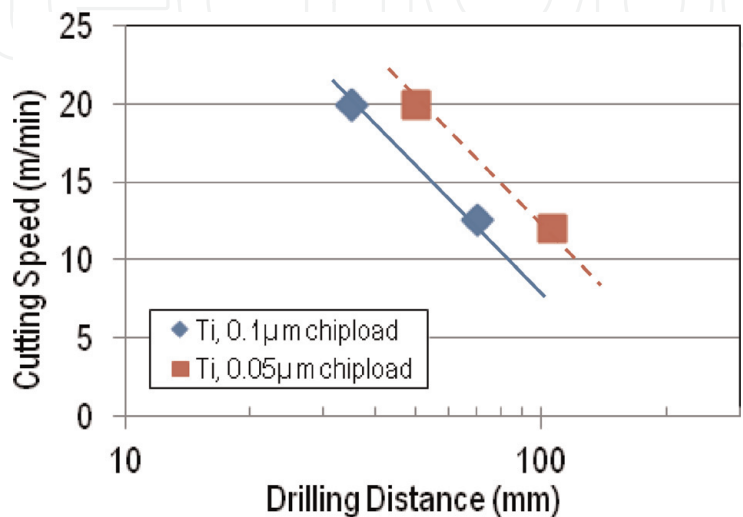


Figure 27.
Tool life plot for microdrilling of CP titanium. Progressive pecking, tool life criterion 8 μm [28].

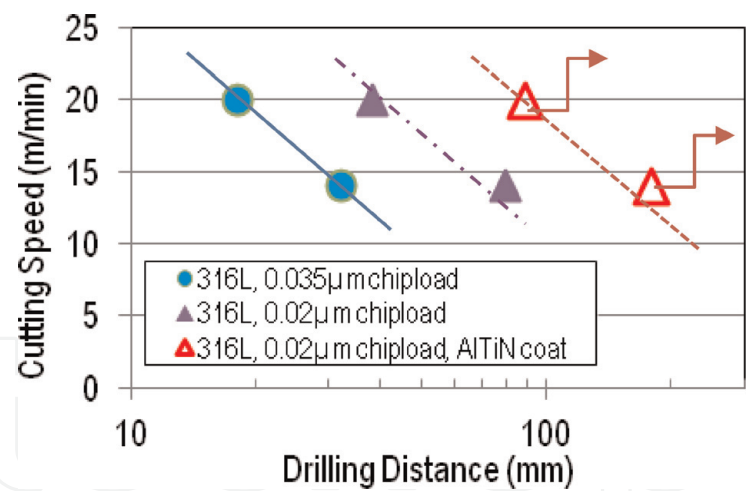


Figure 28. Tool life plot for microdrilling of 316L stainless steel. Progressive pecking, tool life criterion 15 μm . Drilling with AlTiN coated drills were stopped due to shortage of materials [28].

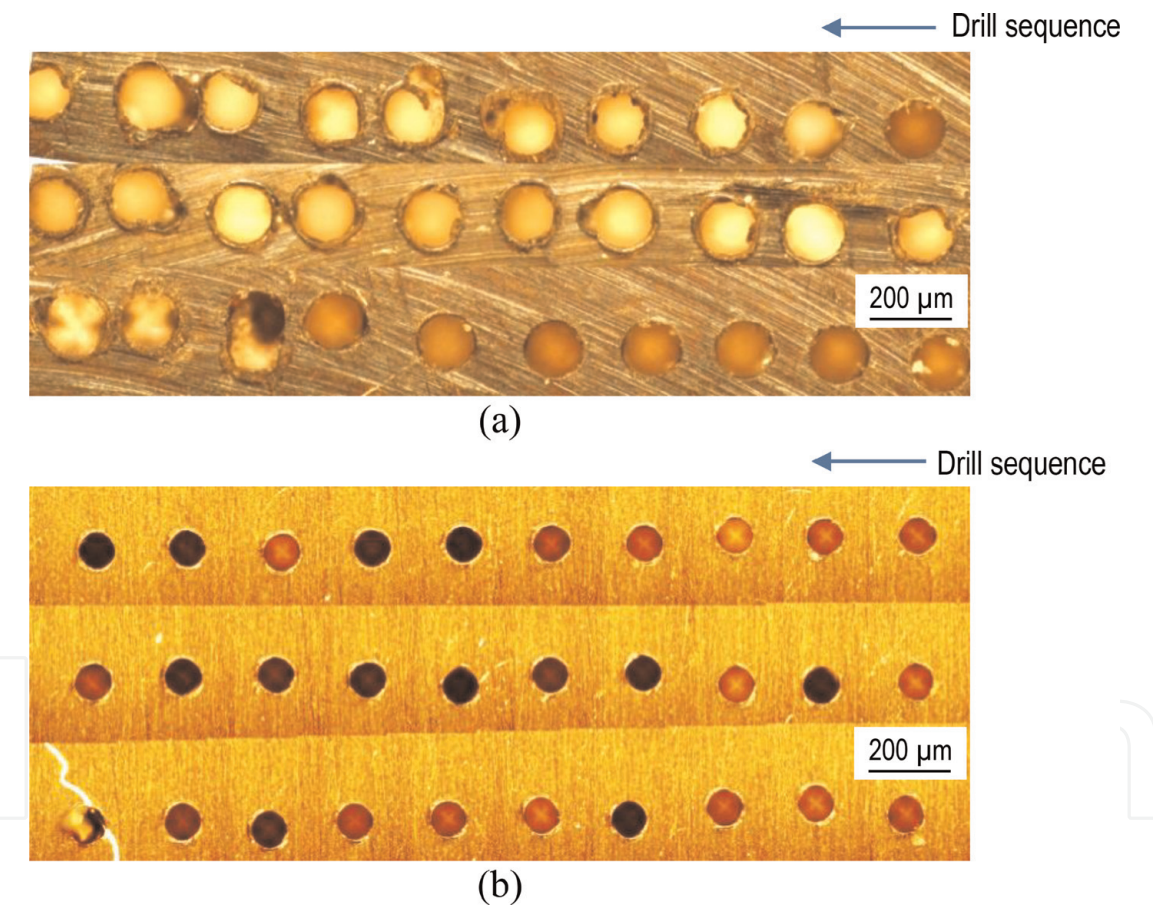


Figure 29. Composite optical images showing drill wandering and hole accuracy on (a) milled CP titanium surface; 4 m/min, 1 $\mu\text{m}/\text{flute}$, 2:1 aspect ratio, and (b) polished CP titanium surface; 12 m/min, 0.05 $\mu\text{m}/\text{flute}$, 10:1 aspect ratio [28].

surface by a worn tool, and smearing of BUE on the drill wall. Similar work hardening effect is reported while drilling austenitic stainless steel leading to a higher resistance near the chisel edge of the drill. Ideally, the drill cutting edges should not shear the workpiece within the work hardened layer from a previous cut. Since the work hardening zone is about 30 μm , it is impractical to microdrill 316L stainless steel at an aggressive chip load more than 30 $\mu\text{m}/\text{flute}$ since a fragile microdrill would simply fracture.

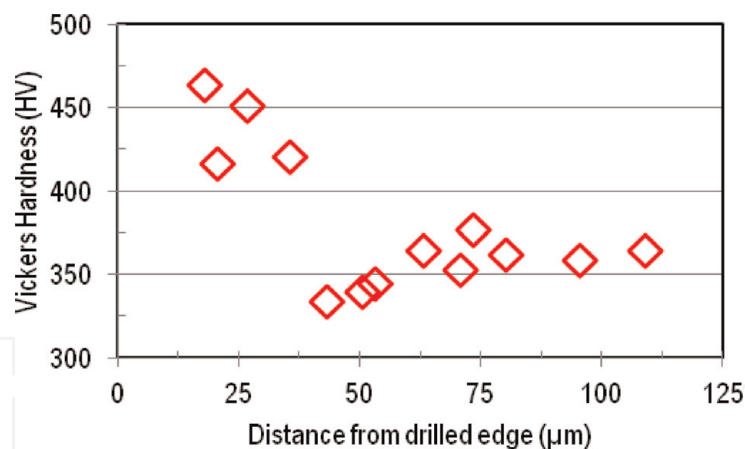


Figure 30.
 Vickers microhardness below drilled surface of the 10th hole. 12.7 mm drilling distance, 14 m/min, 0.035 μm/flute chip load on 316L stainless steel. Microhardness test at 50 g load, 14 s dwell time [28].

4.3 Ultraprecision turning

Product miniaturization and demand for ultraprecision products drives the rapid development of micro/nano scale turning or ultraprecision turning. This technology produces polished and high quality spherical, aspherical parts from metals, ceramics, semiconductors, and polymers that cannot be economically produced by traditional grinding, lapping, or polishing processes. Micro/nano turning also produces intricate shape with low or no subsurface damage since it operates in the ductile-regime mode.

Commercial lathe systems for ultraprecision machining are available. Although tool and axes motions can be in the nanometer ranges, it is an engineering challenge to control the thermal drift issue of a large system. Having a very compact 200-mm system, however, would compromise the required resolution for precision microturning [29]. Diamonds are commonly used for micro/nano turning. Polycrystalline diamond tools are sintered from micron-sized diamond grains. It is less expensive but with limited capability due to large edge radius (few hundred nanometers) and lower edge strength due to attrition wear. Single crystalline diamond tools are best for micro/nano turning since they:

- Have single crystalline structure that allows a sharp cutting edge as small as few nanometers (**Figure 1b**),
- Have highest thermal conductivity among all engineering materials,
- Retain high strength and hardness at high temperature,
- Possess high elastic and shear moduli to resist plastic deformation, and
- Exhibit a low coefficient of friction.

A diamond tool, however, is costly and brittle. A tool with zero or negative rake angle (i) improves its edge strength, and (ii) forms a hydrostatic compressive stress field in the material just in front and below a tool, therefore, minimizes crack initiation. The single crystal diamond typically has (110) crystal plane as rake face and is brazed onto a steel shank of different shape and size.

Not any material can be successfully micro/nano turned with a diamond tool. Ferrous alloys and silicon carbide (SiC) are not suitable for diamond turning

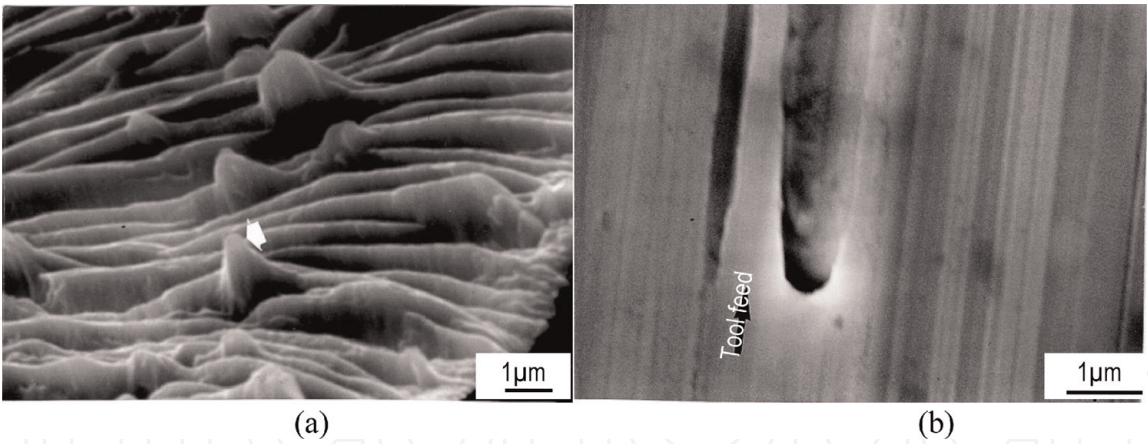


Figure 31.
(a) Microchip from CA 173 showing a beryllide inclusion, (b) deep scratch on machined surface by a broken beryllide.

because of diffusion from highly concentrated carbon in diamond tool to a lower concentration zone of carbon in workpiece materials when the cutting zone is at high temperature during machining. Selected materials that can be successfully machined with a diamond tool are shown in **Table 4**. These material should be homogeneous and contain few if no impurities. The hard inclusions might either damage a sharp diamond edge or being sheared off and smearing against the machined surface. **Figure 31** shows the hard beryllides in beryllium copper CA173 that plow and smear the mirror finish surface.

Semiconductor	Metal	Ceramic	Plastics
Cadmium telluride	Aluminum alloys	Aluminum oxide	Acrylic
Gallium arsenide	Copper alloys	Zirconium oxide	Fluoroplastics
Germanium	Electroless nickel	Optical glasses	Nylon
Lithium niobate	Gold	Quartz	Polycarbonate
Silicon	Magnesium		Polymethylmethacrylate
Silicon nitride	Silver		Propylene
Zinc selenide	Zinc		Styrene
Zinc sulphide			

Table 4.
Examples of diamond machinable materials.

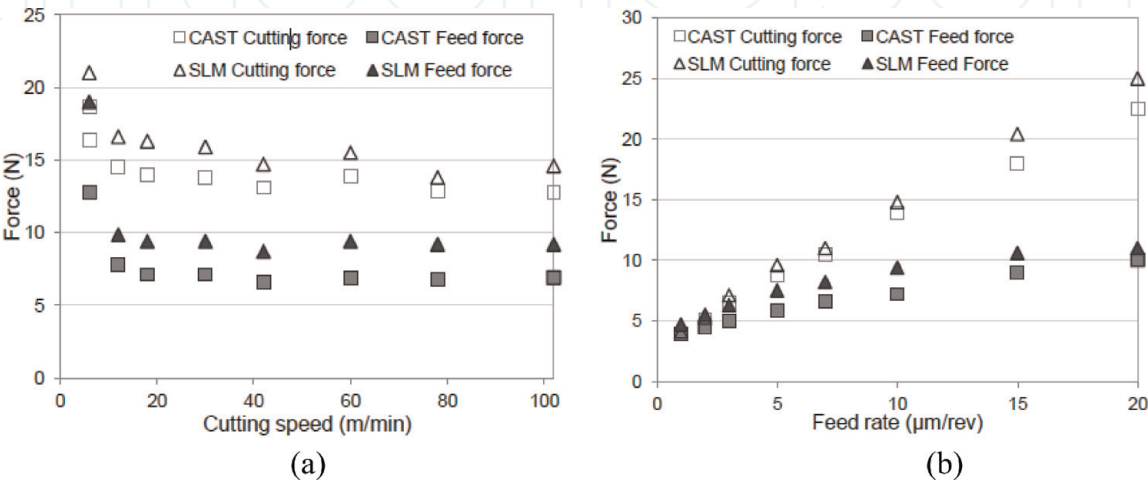


Figure 32.
Comparison of cutting forces in orthogonal microturning of cast and selective laser melted Ti 6Al 4V [30].

Micromist is required to lubricate and cool both tool and machined surface. A micromist nozzle should move with a tool while blowing micro/nano chips away from the machined surface.

An experimental study was done to compare machinability of Ti 6Al 4V produced by casting or selective laser melting. TiAlN coated microturning tools with 8° rake angle, 1.3 µm edge radius were used. Microturning at orthogonal condition was performed at 6–600 m/min, 1–20 µm/rev, and 500 µm depth of cut. The chip morphologies are similar for both materials and there is no significant effect on microstructure; however, the cutting and feeding forces on AM alloy is about 3–24% higher than those for cast alloy when varying the cutting speed (**Figure 32a**) or changing the feed (**Figure 32b**). Such higher forces would shorten the tool life and subsequently degrade the surface quality.

5. Summary

The demanding for product miniaturization and increasing part precision has fueled the development of micromachining. Recent explosion of product innovation with printing 3D metal parts also escalate the post processing studies due to inherent defects of 3D printed metals. The synergy of subtractive processes—micromilling, microdrilling, and microturning—with additive processes for metals—power bed fusion, material jetting, binder jetting, and direct energy deposition—will enable the successful manufacturing of complex metal parts to meet strict engineering requirement.

Author details


Wayne N.P. Hung^{1*} and Mike Corliss²

¹ Texas A&M University, College Station, Texas, USA

² KGSBO, Katy, Texas, USA

*Address all correspondence to: hung@tamu.edu

IntechOpen

© 2019 The Author(s). Licensee IntechOpen. This chapter is distributed under the terms of the Creative Commons Attribution License (<http://creativecommons.org/licenses/by/3.0>), which permits unrestricted use, distribution, and reproduction in any medium, provided the original work is properly cited. 

References

- [1] Chu WS, Kim CS, Lee HT, Choi JO, Park JI, Song JH, et al. Hybrid manufacturing in micro/nano scale: A review. *International Journal of Precision Engineering and Manufacturing-Green Technology*. 2014;**1**(1):75-92
- [2] Kaynak Y, Kitay O. The effect of post-processing operations on surface characteristics of 316L stainless steel produced by selective laser melting. *Additive Manufacturing*. 2019;**26**:84-93
- [3] Kaynak Y, Tascioglu E. Finish machining-induced surface roughness, microhardness and XRD analysis of selective laser melted Inconel 718 alloy. *Procedia CIRP*. 2018;**71**:500-504
- [4] Jagadesh T, Samual GL. Investigation into cutting forces and surface roughness in micro turning of titanium alloy using coated carbide tool. *Procedia Materials Science*. 2014;**5**:2450-2457
- [5] Afazov AM, Rachev SM, Segal J. Modelling and simulation of micro-milling cutting forces. *Journal of Materials Processing Technology*. 2010; **210**:2154-2162
- [6] Rahim EA. Tool failure modes and wear mechanism of coated carbide tools when drilling Ti-6Al-4V. *International Journal of Precision Technology*. 2007;**1**(1):30-39
- [7] Zhou L, Ni J, He Q. Study on failure mechanism of the coated carbide tool. *International Journal of Refractory Metals and Hard Materials*. 2007;**25**:1-5
- [8] Rutherford KL, Hutchings IM. A micro-abrasive wear test, with particular application to coated systems. *Surface and Coatings Technology*. 1996; **79**:231-239
- [9] Kumar M, Dotson K, Melkote SN. An experimental technique to detect tool–workpiece contact in micromilling. *Journal of Manufacturing Processes*. 2010;**12**:99-105
- [10] Shunmugavel M, Polishetty A, Nomani J, Goldberg M, Littlefair G. Metallurgical and machinability characteristics of wrought and selective laser melted Ti-6Al-4V. *Journal of Metallurgy*. 2016;**2016**:1-10. Article ID 7407918. Available from: <http://dx.doi.org/10.1155/2016/7407918>
- [11] Gu J, Barber G, Tung S, Gu RJ. Tool life and wear mechanism of uncoated and coated milling inserts. *Wear*. 1999; **225–229**:273-284
- [12] Wang Z, Kovvuria V, Araujo A, Bacci M, Hung NP, Bukkapatnam STS. Built-up-edge effects on surface deterioration in micromilling processes. *Journal of Manufacturing Processes*. 2016;**24**:321-327
- [13] Klocke F, Maßmann T, Gerschwiler K. Combination of PVD tool coatings and biodegradable lubricants in metal forming and machining. *Wear*. 2005; **259**:1197-1206
- [14] Nam JS, Kim DH, Chung H, Lee SW. Optimization of environmentally benign micro-drilling process with nanofluid minimum quantity lubrication using response surface methodology and genetic algorithm. *Journal of Cleaner Production*. 2015;**102**: 428-436
- [15] Uzun I, Aslantas K, Bedir F. The effect of minimum quantity lubrication and cryogenic pre-cooling on cutting performance in the micro milling of Inconel 718. *Proceedings of the Institution of Mechanical Engineers, Part B: Journal of*

Engineering Manufacture. 2015;**229**
 (12):2134-2143

[16] Hung NP, Fu YQ. Effect of crystalline orientation in the ductile-regime machining of silicon. *Journal of Advanced Manufacturing Technology*. 2000;**16**:871-876

[17] Kajaria S, Chittipolu S, Adera S, Hung NP. Micromilling in minimum quantity lubrication. *Machining Science and Technology*. 2012;**16**:524-546

[18] Ziberov M, Bacci da Silva M, Jackson M, Hung NP. Effect of cutting fluid on micromilling of Ti-6Al-4V titanium alloy, NAMRC 44-129. *Procedia Manufacturing*. 2016;**5**:332-347

[19] Berestovskyi D, Hung NP, Lomeli P. Surface finish of ball-end milled microchannels. *Micro- and Nano-Manufacturing*. 2014;**2**(0411005):1-10

[20] Rysava Z, Bruschi S. Comparison between EBM and DMLS Ti6Al4V machinability characteristics under dry micro-milling conditions. *Materials Science Forum*. 2016a;**836-837**:177-184

[21] Kuram E, Ozcelik B. Multi-objective optimization using Taguchi based grey relational analysis for micro-milling of Al 7075 material with ball nose end mill. *Measurement*. 2013;**46**:1849-1864

[22] Sadiq M, Hoang MN, Valencia N, Obeidat S, Hung NP. Experimental study of micromilling selective laser melted Inconel 718 superalloy. *Procedia Manufacturing*. 2018;**26**:983-992

[23] Vazquez E, Gomar J, Ciurana J, Rodríguez CA. Analyzing effects of cooling and lubrication conditions in micromilling of Ti6Al4V. *Journal of Cleaner Production*. 2015;**87**:906-913

[24] Khan WA, Hoang MN, Tai B, Hung NP. Through-tool minimum quantity lubrication and effect on machinability.

Journal of Manufacturing Processes. 2018;**34**(Part B):750-757

[25] Zhang Y, Jun MBG. Feasibility of lignin as additive in metalworking fluids for micro-milling. *Journal of Manufacturing Processes*. 2014;**16**:503-510

[26] Bruschi S, Tristo G, Rysava Z, Bariani PF, Umbrello D, De Chiffre L. Environmentally clean micromilling of electron beam melted Ti6Al4V. *Journal of Cleaner Production*. 2016;**133**:932-941

[27] Rysava Z, Bruschi S, Carmignato S, Medeossi F, Savio E, Zanini F. Micro-drilling and threading of the Ti6Al4V titanium alloy produced through additive manufacturing. *Procedia CIRP*. 2016b;**46**:583-586

[28] Mohanty S, Wells S, Hung NP. Microdrilling of Biocompatible Materials. IMECE2012-87523, Proceedings, ASME International Mechanical Engineering Congress & Exposition; Houston, Texas. 2012

[29] Lu Z, Yoneyama T. Micro cutting in the micro lathe turning system. *International Journal of Machine Tools and Manufacture*. 1999;**39**:1171-1183

[30] Coz GL, Fischer M, Piquard R, D'Acunto A, Laheurte P, Dudzinski D. Micro cutting of Ti-6Al-4V parts produced by SLM process. *Procedia CIRP*. 2017;**58**:228-232